Journal for ImmunoTherapy of Cancer

Engineered *Mycobacterium smegmatis* expressing anti-PD-L1/IL-15 immunocytokine induces and activates specific antitumor immunity

Yi Mei,[1] Junmeng Zhu,[1] Jie Shao ,[1,2] Lin Li,[1] Fangcen Liu,[1] Xiaoxuan Sha,[1] Yang Yang,[1] Jie Shen ,[1] Rutian Li,[1] Baorui Liu [1]

To cite: Mei Y, Zhu J, Shao J, *et al*. Engineered *Mycobacterium smegmatis* expressing anti-PD-L1/IL-15 immunocytokine induces and activates specific antitumor immunity. *Journal for ImmunoTherapy of Cancer* 2025;**13**:e010118. doi:10.1136/jitc-2024-010118

► Additional supplemental material is published online only. To view, please visit the journal online (https://doi.org/10.1136/jitc-2024-010118).

YM and JZ contributed equally.

Accepted 03 May 2025

[1]Department of Oncology, Nanjing Drum Tower Hospital, Affiliated Hospital of Medical School, School of Life Sciences, Nanjing University, Nanjing, Jiangsu, China
[2]Nanjing University of Chinese Medicine Drum Tower Clinical College, Nanjing, Jiangsu, China

Correspondence to
Dr Baorui Liu;
baoruiliu@nju.edu.cn

ABSTRACT

Background Immune checkpoint inhibitors and cytokines have revolutionized tumor treatment but are still limited by dose-dependent toxicity and efficacy. In situ vaccine platforms based on intelligent microbes are promising therapeutic strategies that sustainably deliver drugs locally without causing severe systemic risks.

Methods In this study, we have innovatively engineered a non-pathogenic, adjuvant-acting *Mycobacterium smegmatis* (*M. smegmatis*) that co-expresses a programmed cell death-ligand 1 (PD-L1) inhibitor and an interleukin-15 (IL-15) cytokine complex containing the interleukin-15 receptor alpha (IL-15Rα) sushi domain (Ms-PDL1scfv-IL15).

Results We demonstrate that the fusion protein of PD-L1 inhibitor and IL-15 cytokine systemically binds mouse or human PD-L1 and maintains IL-15 stimulatory activity. The bifunctional Ms-PDL1scfv-IL15 overcomes resistance to PD-L1 blockade, recruits numerous immune cells in situ, induces dendritic cells (DCs) maturation, initiates the M1 antitumor polarization of macrophages, increases the proliferation and activation of natural killer cells and tumor-infiltrating $CD8^+$ T cells, inhibits regulatory T cells, elicits abscopal effects, stimulates rapid tumor regression, prevents metastasis, and leads to long-term survival in several syngeneic tumor mouse models. We also found that the combination of Ms-PDL1scfv-IL15 with granulocyte-macrophage colony-stimulating factor (GM-CSF) synergistically stunted the tumor progress and stasis. Moreover, intratumoral administration of Ms-PDL1scfv-IL15 can capture tumor antigen fragments, and boost DCs presentation of antigens, which remarkably initiates tumor antigen-specific immune response, leading to durable tumor regression and specific antitumor immunity.

Conclusion In summary, the engineered *M. smegmatis* can recruit and activate innate and adaptive antitumor immune responses, offering a potent cancer immunotherapy strategy to treat patients with cold tumors or resistance to checkpoint blockade.

WHAT IS ALREADY KNOWN ON THIS TOPIC

⇒ The combination of immune checkpoint inhibitors and cytokines represents a promising approach for antitumor immunotherapy. However, its efficacy is constrained by immune resistance and dose-dependent toxicity. To overcome these limitations, locally sustainable drug delivery systems based on intelligent microbes have emerged as an effective strategy.

WHAT THIS STUDY ADDS

⇒ *Mycobacterium smegmatis* (*M. smegmatis*) co-expresses programmed cell death-ligand 1 (PD-L1) antibody and interleukin-15 (IL-15) cytokine, facilitating sustained delivery of the molecule to the tumor site and eliciting both innate and specific antitumor immune responses.

HOW THIS STUDY MIGHT AFFECT RESEARCH, PRACTICE OR POLICY

⇒ Our study provides new opportunities for the development of PD-L1 antibody and IL-15 cytokine-modified *M. smegmatis* as therapeutic agents for malignancies. To provide a potential cancer immunotherapy strategy to treat patients with cold tumors or resistance to checkpoint blockade.

INTRODUCTION

Immune checkpoint inhibitors and cytokines have revolutionized the paradigm of cancer immunotherapy and are commonly used as therapeutic strategies for in situ vaccines.[1–4] Programmed cell death-ligand 1 (PD-L1) antibody and interleukin-15 (IL-15) cytokine have shown promising effects in treating several cancers. However, serious immune-related adverse effects can be caused, which limits their application.[5–7] From a detailed perspective, IL-15 cytokine has a short half-life, limited biological activity, and dose-limiting toxicity in vivo,[8–11] while high-dose PD-L1 antibody is prone to triggering a storm of inflammatory cytokines.[5 6 12 13] In addition, although the combination therapy of anti-PD-L1/anti-programmed cell death protein 1 (anti-PD-1) and IL-15 is more effective than single therapy regimens, the combination therapy tends to cause higher-grade toxicity,

which is difficult for patients to tolerate even if the effect is better.[14] Thus, there is an urgent need to develop new delivery platforms for immune checkpoint inhibitors and cytokines that can circumvent these limitations and provide safer, more effective, and minimally invasive treatment options.

Recent studies have revealed that several microorganisms play an important role in reprogramming the tumor immune microenvironment, modulating tumor development and progression.[15–18] With the progress of synthetic biology, bacteria provide a natural platform as an intelligent microbial delivery system.[19 20] *Bacillus Calmette Guerin* (*BCG*), an important component of Complete Freund's adjuvant,[21] is currently the only live bacterial biological agent approved by the Food and Drug Administration (FDA) for the treatment of bladder cancer.[22 23] *Mycobacterium smegmatis (M. smegmatis)*, a non-pathogenic microorganism belonging to *Mycobacterium* species, is similar to *BCG*, which can act as an immune adjuvant with no endotoxin.[24–26] The potential of *M. smegmatis* in cancer immunotherapy has been overlooked due to the lack and limitation of genetic manipulation tools.[27] In addition, compared with *BCG*, *M. smegmatis* is more susceptible to damage by phagolysosomal proteases in the phagosomes of infected cells, which can promote the better release of therapeutic substances, inducing the maturation of dendritic cells (DCs) and better cross-presentation of antigens to T cells.[28–30]

Here, we designed a genetically engineered *M. smegmatis* as an in situ vaccine. Specifically, we first screened suitable α-antigen signal peptides (Accession numbers: M21839 in the National Center for Biotechnology Information (NCBI)] databank) for the continuous secretion of the fusion protein comprizing PD-L1 inhibitor and IL-15 cytokine. While blocking the immune escape of tumor cells, Ms-PDL1scfv-IL15 activated macrophages, DCs, and natural killer (NK) cells, inducing $CD8^+$ T cell proliferation in situ and converting the "cold" tumors to "hot" tumors. Combination therapy with Ms-PDL1scfv-IL15 and granulocyte-macrophage colony-stimulating factor (GM-CSF) exerts synergistic antitumor effects in the colorectal model. In addition, the engineered *M. smegmatis* can capture antigen fragments during tumor regression. Tumor antigens attached to Ms-PDL1scfv-IL15 will boost more effective presentation of antigens by DCs and initiate tumor antigen-specific immune responses.

RESULTS

Generation and characterization of bacteria co-expressing a fusion protein of PD-L1 inhibitor and IL-15 cytokine (Ms-PDL1scfv-IL15)

A single-chain variable fragment (scfv) blocking PD-L1 was chosen from the Research Collaboratory for Structural Bioinformatics Protein Data Bank (RCSB PDB), and an IL-15 cytokine containing the interleukin-15 receptor alpha (IL-15Rα) sushi domain was opted as therapeutic immune activator.[31] We first hypothesized that *M. smegmatis* releasing PD-L1 inhibitor and IL-15 fusion protein in tumors would promote infiltration of activated T cells and enhance antitumor immunity (figure 1a). Toward this aim, we first engineered *M. smegmatis* to express the scfv fragment of PD-L1 inhibitor fused with a FLAG (a synthetic epitope tag system, DYKDDDDK) tag (Ms-PDL1scfv) to screen out a better signal peptide. We compared the α-antigen signal peptide sequence of *M. smegmatis* and *BCG*,[32] and found that the latter had stronger secretory ability under the same conditions (online supplemental figure 1a). Next, we successfully generated a constitutive vector containing α-antigen signal peptide of *BCG* and hsp60 strong promoter, as indicated by western blot analysis with FLAG tag antibody and IL-15 antibody (figure 1b,c). Using flow cytometry, we first tested the binding ability of PDL1scfv. We incubated human malignant melanoma cells A375 and mouse colon cancer cells MC38 with culture medium supernatants and bacterial lysates containing PD-L1scfv, and then detected the binding ability by constant concentration of fluorescence-conjugated anti-PD-L1 monoclonal antibody. The findings demonstrated that both Ms-PDL1scfv and MS-PDL1scFV-IL15 exhibited specific binding to the epitope of anti-PD-L1 monoclonal antibody through competitive interaction (figure 1d). We also directly detected that PD-L1scfv could bind to PD-L1 on the target cell surface by fluorescently conjugated Flag antibody, and the binding effect was not significantly different from that of commercial PD-L1 monoclonal antibody (online supplemental figure 1b). We then measured the concentration of IL-15 in the culture medium and the serum by ELISA kit (figure 1f, online supplemental figure 1c). To examine the ability of IL-15 to promote T cell activation and proliferation, the engineered bacteria were co-incubated with carboxyfluorescein diacetate succinimidyl ester (CFSE) labeled T cells for 5 days. Flow cytometry analysis showed that engineered IL-15 significantly promoted the activation and proliferation of T cells, whereas engineered PDL1scfv showed a limited increase (figure 1e). In the cell counting kit 8 assay, the ability of IL-15 to promote the proliferation and activation of T cells was further detected by incubation with different diluted concentrations of engineered bacteria and T cells. As shown in figure 1g,h, Ms-PDL1scfv-IL15 and Ms-IL15 exhibited strong proliferative capacity in human and mouse T cells, the proliferation rate of human and mouse T cells in the Ms-PDL1scfv-IL15 group was 2.77-fold and 1.18-fold higher than that in the Ms-IL15 group, respectively. This result is consistent with the result of figure 1e. Taken together, these data demonstrate that Ms-PDL1scfv-IL15 can produce and secrete high levels of functional PD-L1scfv and IL-15 cytokine.

We also examined the growth patterns of the engineered bacteria to assess any potential impact on their strain characteristics. Specifically, we examined the growth pattern of these bacteria in the culture medium and observed no significant differences among the three engineered strains (online supplemental figure

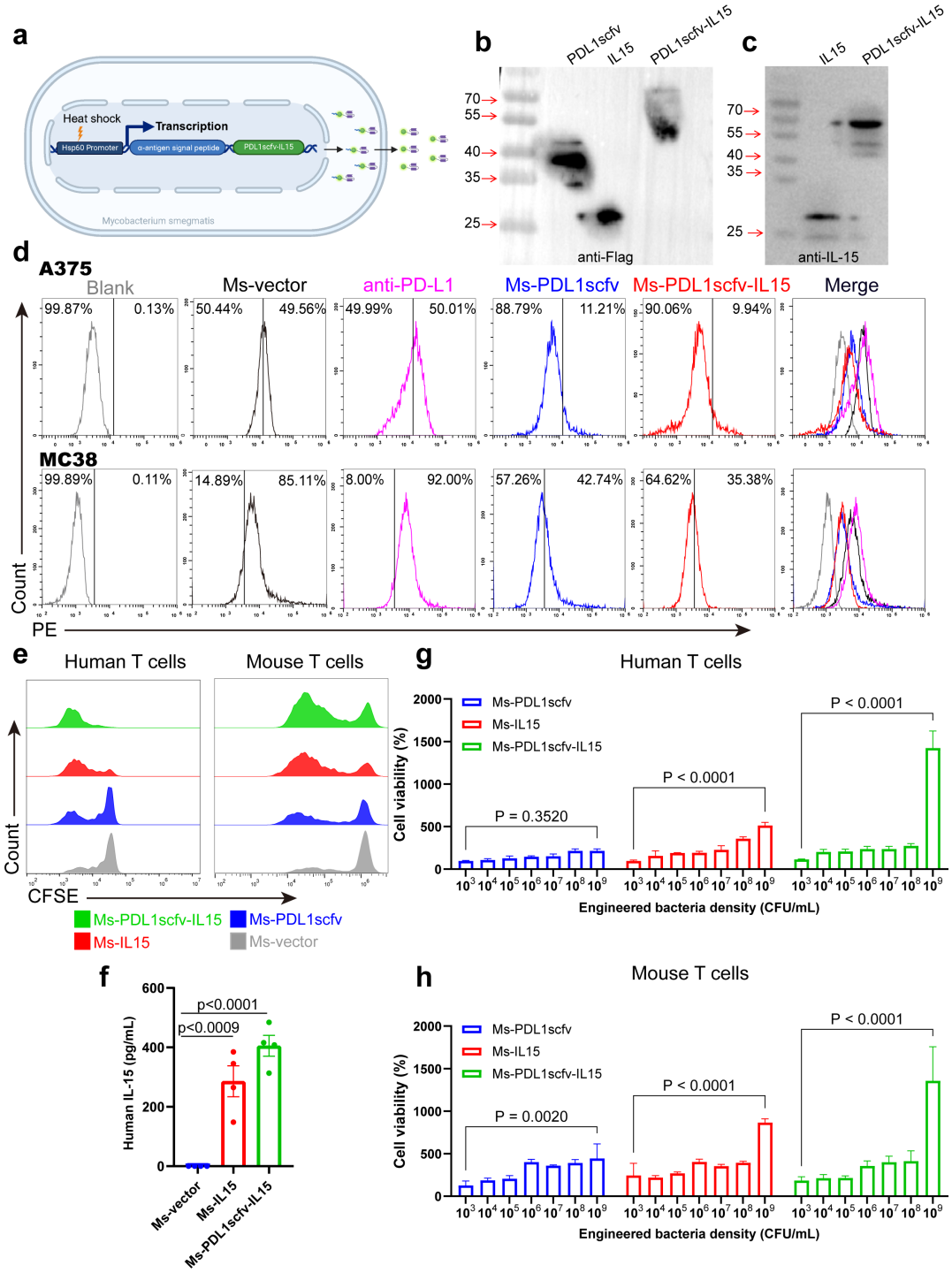

Figure 1 Generation and characterization of engineered *M. smegmatis* delivering PDL1scfv-IL15 fusion protein (Ms-PDL1scfv-IL15). (a) A schematic diagram of engineered *M. smegmatis* shuttle vectors expressing PDL1scfv and/or IL15 by α-antigen signal peptide secretion. (b, c) Expression and secretion of PDL1scfv or/and IL15 from recombinant *M. smegmatis* with the indicated anti-Flag (b) or anti-IL-15 (c) was used for western blot. The experiment was repeated twice. (d) Flow cytometry was used to analyze the binding ability of PDL1scfv to PD-L1 epitopes in A375 and MC38 cells by competing epitopes. Tumor cells were incubated with culture medium supernatants and bacterial lysates containing PD-L1scfv for 2 hours. Tumor cells were harvested and subjected to flow cytometry using a commercial PD-L1 antibody labeled with PE fluorescence. (e) Human or mouse T cells were stained with CFSE and incubated with 1×10^8 CFU/mL engineered bacteria for 5 days before T cell proliferation was measured by flow cytometry. (f) The culture medium supernatant of engineered bacteria (1×10^8 CFU) was collected. The amount of the target protein in the supernatant was assessed by ELISA (n=4, biologically independent samples). (g, h) Human or mouse T cell proliferation stimulated by Ms-PDL1scfv, Ms-IL15, or Ms-PDL1scfv-IL15. The data are shown as the mean±SD of triplicate samples. Results generated by three technical repeats of each experimental method. CFSE, carboxyfluorescein diacetate succinimidyl ester; CFU, colony-forming unit; IL-15, nterleukin-15; *M. smegmatis*, *Mycobacterium smegmatis;* PE, phycoerythrin; PD-L1, programmed cell death-ligand 1.

2a). Subsequently, when various concentrations of these engineered bacteria were incubated with phagocytes and tumor cells in vitro, we noted an initial expansion followed by a subsequent decline (online supplemental figure 2b–f). This phenomenon could be attributed to phagocyte clearance or nutrient depletion within the culture medium leading to bacterial death. However, no notable distinctions were observed between different engineered strains. In summary, our findings demonstrate that there were no substantial variations among the engineered bacteria.

Ms-PDL1scfv-IL15 efficiently induced the activation of DCs and T cells in vitro

M. smegmatis has been reported to promote the internalization and specific recognition of therapeutic drugs or antigens by DCs, thereby better promoting the efficient cross-presentation of foreign antigens to T cells.[33] Therefore, we examined the internalization of Ms-PDL1scfv-IL15 by bone marrow-derived DCs (BMDCs). The engineered bacteria were labeled with the membrane dye DiO and the BMDCs were labeled with DiI for visualization. After co-incubation for 24 hours, it was clearly found that the bacteria were captured and engulfed by BMDCs (figure 2a), and certain bacterial membranes remained incompletely metabolized even after a week (online supplemental figure 3).

To evaluate the DCs activation, different concentrations of engineered bacteria were incubated with BMDCs for 24 hours in vitro. Phosphate-buffered saline (PBS) and lipopolysaccharide (LPS) were used as negative and positive controls, respectively. The results demonstrated that engineered bacteria could effectively stimulate the activation of BMDCs in a dose-dependent manner. There was a significant increase in the percentage of mature DCs ($CD80^+$ $CD86^+$) in the Ms-PDL1scfv-IL15 group within the concentration range of 10^5–10^9 colony-forming unit/mL (CFU/mL), even much better than the LPS group (44.57%). When the concentration of Ms-PDL1scfv-IL15 reached 10^9 CFU/mL, the average maturation proportion of BMDCs reached 57.53%. The other two strains of engineered bacteria also effectively induce the activation of BMDCs in a dose-dependent manner, which is not significantly different from the Ms-PDL1scfv-IL15 group (figure 2b). The possible explanation is that the activation of BMDCs is most likely due to the stimulation of the innate immune response caused by bacteria. To determine whether the engineered bacteria could directly induce tumor cell death, MC38 cells were incubated with different concentrations of Ms-PDL1scfv-IL15 for 24 hours, and the cell viability was measured by staining with propidium iodide, a cell impermeable dye that stains cells that have lost membrane integrity. The results showed that when the concentration of bacteria reached 10^{10} CFU/mL, the viability of cells was significantly decreased compared with the PBS group, which also suggested that too high a concentration of bacteria may be accompanied by a cytotoxic effect (figure 2d). Therefore, we selected the concentration of 10^9 CFU/mL as the following experimental concentration based on the efficacy and safety considerations. Furthermore, we examined the capacity of Ms-PDL1scfv-IL15 to stimulate T cell activation, and proliferation, enhancing their cytotoxic activity.

We next examined the ability of the engineered bacteria to induce T cell cytotoxicity at different effector-target ratios (E:T). We found that the cell mortality rate of the Ms-PDL1scfv-IL15 group increased from 10.33% to 15.35% compared with the control group at the E:T of 1:10:100, and the cytotoxic effect was further improved by increasing the ratio of effector to target (figure 2c). However, both Ms-PDL1scfv and Ms-IL15 exhibited significantly reduced potency in inducing T cell cytotoxicity, with Ms-PDL1scfv demonstrating a complete lack of induction capability (online supplemental figure 4a). Meanwhile, the secretion of interferon-γ (IFN-γ), tumor necrosis factor-α (TNF-α), IL-6, IL-2, IL-4, and IL-13 significantly increased in the Ms-PDL1scfv-IL15 group compared with the other groups, which played crucial roles in the initiation and stimulation of innate immune response (figure 2e–j). Furthermore, a significantly elevated expression of the CD69 marker on T cells was observed in the Ms-PDL1scfv group compared with the other experimental groups, providing compelling evidence for the efficacy of engineered bacteria in inducing robust T cell activation (figure 2k, online supplemental figure 4b).

Microbial spatial and temporal distribution of Ms-PDL1scfv-IL15

Engineered bacteria have been applied to the local therapeutic modality of various cancers due to their attractive tumor-targeting and continuous generation of therapeutic cargo.[34] *M. smegmatis* cannot move freely in the tumor microenvironment due to the lack of flagella,[35] which further strengthens the above characteristics after intratumoral (i.t.) injection. To confirm the spatial and temporal distribution of bacteria in vivo, we injected DiR-labeled bacteria intratumorally once to visualize the distribution of Ms-PDL1scfv-IL15. All injected bacteria were found to accumulate in the tumor microenvironment, which peaked at 72 hours and then gradually decreased with the prolongation of treatment time (figure 3a). Tumors and tumor-draining lymph nodes (TDLNs) were resected at different time points (6, 24, 72, 168, 336 hours) and measured ex vivo, and the results were consistent with those in vivo (figure 3b–d). Interestingly, we found that the fluorescence was also detected in the TDLN, which might provide an excellent opportunity for immune activation, which may be related to the homing movement of immune cells to TDLN after exerting phagocytic function. In addition, there was almost no fluorescence signal in other organs such as heart, liver, spleen, lung, and kidney (online supplemental figure 5), indicating good biosafety of local administration of Ms-PDL1scfv-IL15. Similar results were shown by the in vitro

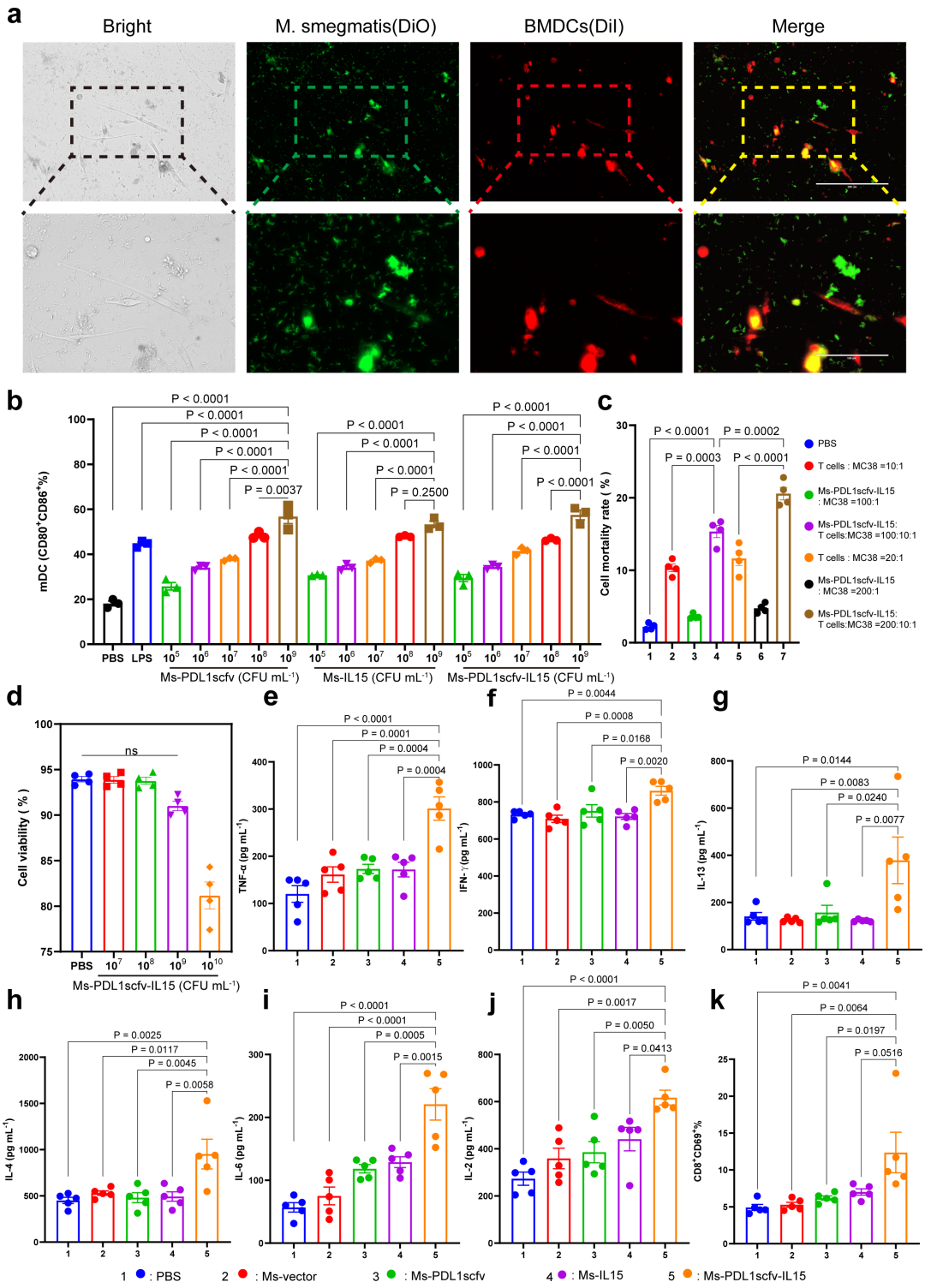

Figure 2 Ms-PDL1scfv-IL15 efficiently induced the activation of DCs and T cells in vitro. (a) Colocalization analysis of Ms-PDL1scfv-IL15 (DiO, green) in bone marrow-derived DCs (BMDCs) (DiI, red) after 24 hours incubation by confocal microscopy (one representative data was shown from three independently repeated experiments). White scale bars: up, 200 µm; down, 100 µm. (b) The percentage of mature DCs (mDCs, $CD11c^+$ $CD80^+$ $CD86^+$) after co-incubation with engineered bacteria in vitro for 24 hours (n=3, biologically independent samples). (c) Ms-PDL1scfv-IL15, T cells, and MC38 cells were incubated at different ratios of effector to target for 24 hours to induce T cell cytotoxicity (n=4, biologically independent samples). (d) The cell viability of MC38 cells after co-incubation with Ms-PDL1scfv-IL15 in vitro for 24 hours (n=4, biologically independent samples). (e–j) In vitro assessment of pro-inflammatory cytokines in co-culture supernatants following 24 hours stimulation of T cells with engineered bacteria (n=5, biologically independent samples). (k) The quantification of CD69 expression on $CD8^+$ T cell subsets in the T cells (n=5, biologically independent samples). CFU, colony-forming unit; DCs, dendritic cells; IL, interleukin; IFN, interferon; LPS, lipopolysaccharide; *M. smegmatis*, *Mycobacterium smegmatis;* PBS, phosphate-buffered saline; TNF, tumor necrosis factor.

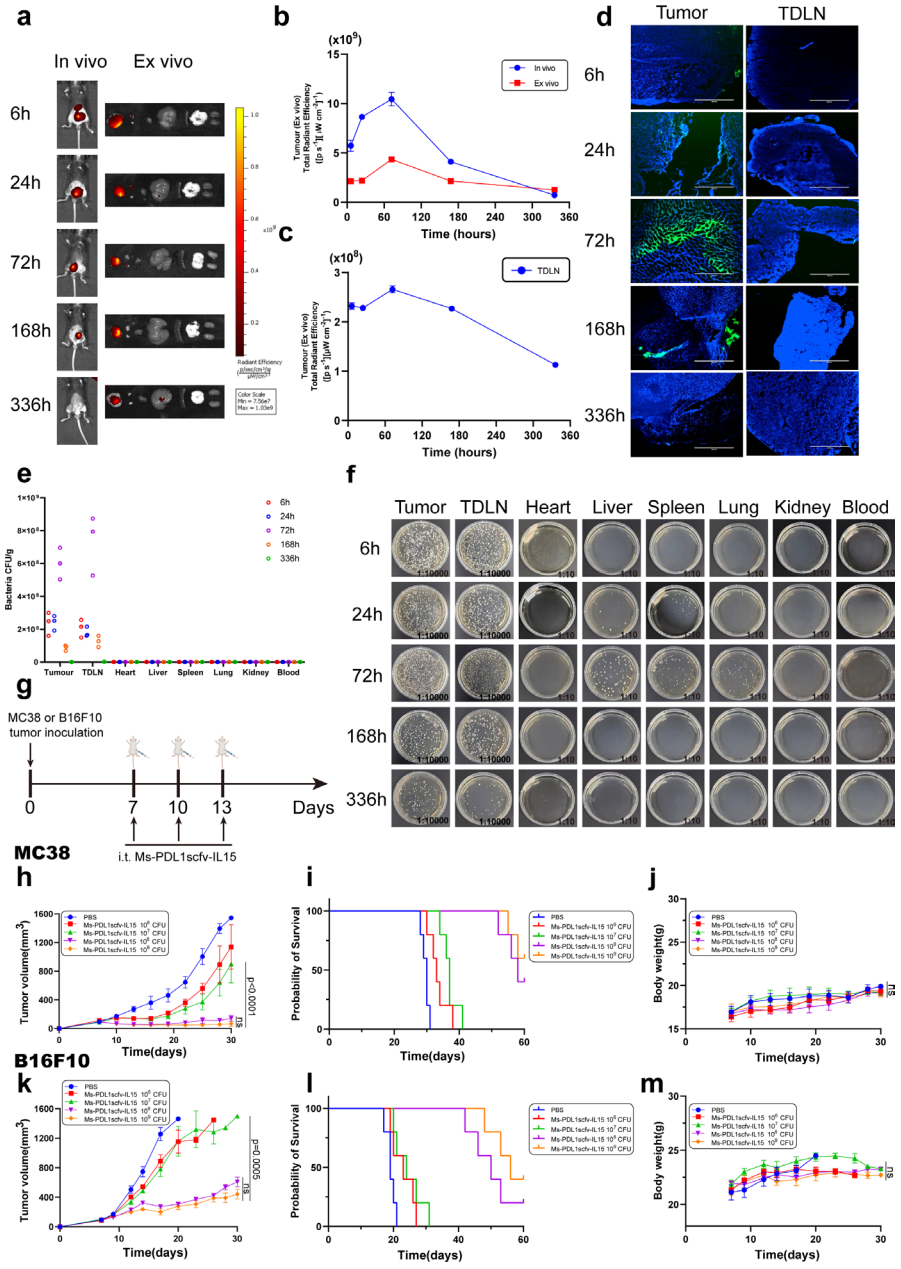

Figure 3 Microbial spatial and temporal distribution of Ms-PDL1scfv-IL15. (a) Representative in vivo near-infrared imaging of tumor-bearing mice at 6, 24, 72, 168, 336 hours after intratumoral injection of 10^8 CFU Ms-PDL1scfv-IL15 (n=3), and representative ex vivo images of the tumors, TDLNs, hearts, livers, spleens, lungs, and kidneys, collected at 6, 24, 72, 168, 336 hours after injection (n=3). (b, c) Total radiant efficiency of Ms-PDL1scfv-IL15 signal in tumors in vivo or ex vivo over time (n=3, biologically independent samples). The error bars represented mean±SEM. (d) Frozen sections of tumors and TDLNs in the MC38 mouse colon tumor model at 6, 24, 72, 168, 336 hours after intratumoral injection of 10^8 CFU Ms-PDL1scfv-IL15 (n=3). Ms-PDL1scfv-IL15 were labeled with DiO (green); nucleus, blue. White scale bars, 1,000 µm. (e, f) Representative photographs of solid 7H10 agar plates (f) and quantification (e) of bacterial colonization in various organs harvested from MC38-bearing mice at different time points after intratumoral injection of 108 CFU Ms-PDL1scfv-IL15 (n=3, biologically independent samples). (g) Schematic diagram of the treatment in MC38 or B16F10 tumor-bearing mice. C57BL/6 mice were subcutaneously implanted with MC38 cells (2×10^6/per) or B16F10 cells (5×10^5/per) on the left lower sides of the abdomen on day 0, and received treatments on days 7, 10 and 13. (h–j) C57BL/6 mice were subcutaneously inoculated with MC38 cells. When tumor sizes reached~100 mm^3, the mice were intratumorally injected with 100 µL of 10^6 CFU, 10^7 CFU, 10^8 CFU, 10^9 CFU Ms-PDL1scfv-IL15 or PBS on days 7, 10, and 13. (h) Caliper measurement of MC38 tumor were performed on the indicated days (n=5). The error bars represented mean±SEM. P values were calculated by two-way ANOVA and Tukey post-test and correction, ns, not significant. (i) Survival curves of MC38 tumor mice in different groups for 60 days (n=5). (j) Average weight of different groups for 30 days (n=5). The error bars represented mean±SEM, p values were calculated by two-tailed unpaired Student's t-tests, ns, not significant. (k–m) Tumor volume (k), survival curves (l) and average weight (m) of the B16F10 tumor model was monitored using the same treatment schedule as in (h–j). ANOVA, analysis of variance; CFU, colony-forming unit; PBS, phosphate-buffered saline; TDLN, tumor-draining lymph nodes.

agarose plate spreading method (figure 3e,f). Meanwhile, the engineered bacteria were observed to be completely cleared from the system within 672 hours (online supplemental figure 6a–c).

To determine the optimal concentration of Ms-PDL1scfv-IL15 for i.t. injection, we subcutaneously implanted MC38 or B16F10 tumor cells in C57BL/6 mice. When established tumors were palpable (~100 mm^3), different concentrations of Ms-PDL1scfv-IL15 dissolved in 100 µL PBS were injected locally (figure 3g). The tumor growth of the 10^8 CFU group and 10^9 CFU group was greatly inhibited compared with the other three groups of PBS, 10^6 CFU, and 10^7 CFU (figure 3h,k). Consistently, the survival of mice in the 10^8 CFU group and 10^9 CFU group was significantly longer than that of any other group (figure 3i,j). Based on the biological burden and therapeutic efficacy, we finally treated mice with 10^8 CFU Ms-PDL1scfv-IL15, and different concentrations of treatment doses did not cause sudden changes in the body weight of mice (figure 3j,m).

Ms-PDL1scfv-IL15 elicits in vivo tumor suppression

We examined the efficacy of Ms-PDL1scfv-IL15 in vivo after we determined the effective concentration. We first tested the antitumor effect of Ms-PDL1scfv-IL15 in the MC38 cell colon cancer model, performing intratumoral injections of bacteria every 3 days for a total of three treatments, with multiple injections performed to maintain the highest bacterial concentration and minimize the likelihood of plasmid loss (figure 4a). In fact, we also assessed the plasmid retention rate of three engineered strains prior to intratumoral injection, revealing a plasmid retention rate exceeding 90% (online supplemental figure 6d). Significant reductions in tumor growth were observed in mice treated with Ms-PDL1scfv-IL15 as compared with those treated with PBS, *M. smegmatis* with empty vectors (Ms-vector), Ms-PDL1scfv or Ms-IL15 (figure 4b), confirming the therapeutic activity of *M. smegmatis*-mediated intratumoral delivery of PDL1scfv inhibitor and IL-15 fusion protein in vivo. Notably, the Ms-PDL1scfv-IL15 induced complete regression (CR) in two out of seven MC38 tumor-bearing mice (figure 4e,h). Suppression of the tumors resulted in prolonged survival of the mice in the Ms-PDL1scfv-IL15 group, and 60% of mice in the Ms-PDL1scfv-IL15 group survived for 60 days (figure 4c). The body weight change in all groups had a similar changing pattern during the treatment (figure 4d). Meanwhile, we were surprised to find that the TDLN (figure 4f,i) and spleen (figure 4g,j), which serve as sources of DCs and T cells, were larger and heavier in the Ms-PDL1scfv-IL15 group than those in the other groups, suggesting that intense antitumor immune activity occurs in vivo.

We want to know if the live bacteria are actually required for the observed tumor control. Using the same treatment strategy (online supplemental figure 7a), we also conducted additional experiments with PDL1scfv-IL15 Protein group, Ms-PDL1scfv-IL15 Lysate group, and Inactivated Ms-PDL1scfv-IL15 group. The results showed that the treatment with the protein alone had some ability to control tumors, but the treatment effect was more pronounced when bacteria were added (online supplemental figure 7b,c). This may be related to the fact that bacteria can activate the innate immune system.[36] In addition, the treatment effect of live bacteria treatment is the most significant, which may be related to the fact that Ms-PDL1scfv-IL15 can deliver drugs locally sustainably without causing severe systemic risks.

Ms-PDL1scfv-IL15 induces both innate and adaptive immune cell activation in tumors

To assess the specific immune response in the immune microenvironment, we removed intratumorally treated tumors, TDLNs, and spleens of mice in the five groups after 7 days from the last treatment to detect the changes in tumor-infiltrating lymphocytes.

The in situ vaccine effect caused by Ms-PDL1scfv-IL15 induced a large number of mature DCs in tumors, both CD80 and CD86 exhibited increased geometric mean fluorescence intensity (MFI), indicating a more mature state of DCs (figure 5f,g), among which the functional $CD11c^+CD103^+$ DCs were even increased by 1.7-fold compared with the PBS group (figure 5h), indicating that the Ms-PDL1scfv-IL15 was a critical factor in improving the cross-presentation ability of DCs. Phenotyping of tumor-infiltrating lymphocytes revealed that the Ms-PDL1scfv-IL15 induced an increase in activated and proliferating $CD3^+CD8^+$ and $CD3^+CD4^+$ T cells (figure 5d,e). The proportion of effector memory T cells (Tem, $CD3^+$ $CD8^+$ $CD44^+$ $CD62L^-$) subset increased to more than 20% (figure 5a), and no significant differences were observed in the proportion of central memory T cells (Tcm, $CD3^+$ $CD8^+$ $CD44^+$ $CD62L^+$) subset during the treatment (figure 5k). In addition, regulatory T cells (Tregs, $CD25^+Foxp3^+/CD4^+$) were significantly decreased in the Ms-PDL1scfv-IL15 group, from 35.30% to 9.31% compared with the PBS group (figure 5b).

In addition to DC and T cell infiltration in tumor tissues, we also studied tumor-associated macrophages (TAMs) and NK cells, which play an important role in innate immunity. The results showed that Ms-PDL1scfv-IL15 could polarize TAMs from immunosuppressive type 2 macrophages (M2, $CD206^+CD163^+/CD11b^+F4/80^+$) to immune-promoting type 1 macrophages (M1, $CD86^+iNOS^+/CD11b^+F4/80^+$). Compared with the PBS group (M2 ratio was 26.13%, M1 ratio was 10.8%), the proportion of M2 in the Ms-PDL1scfv-IL15 group decreased to 8.91%, and the proportion of M1 increased to 23.1% (figure 5c,i). Interestingly, *M. smegmatis* may induce macrophage polarization, and the secreted PD-L1scfv and IL-15 cytokines play a synergistic role. The percentage of NK cells was significantly increased in Ms-PDL1scfv-IL15 and Ms-IL15 groups compared with the PBS group, suggesting that IL-15 cytokine contributes to NK cell proliferation and infiltration (figure 5j), which is consistent with previous reports.[37]

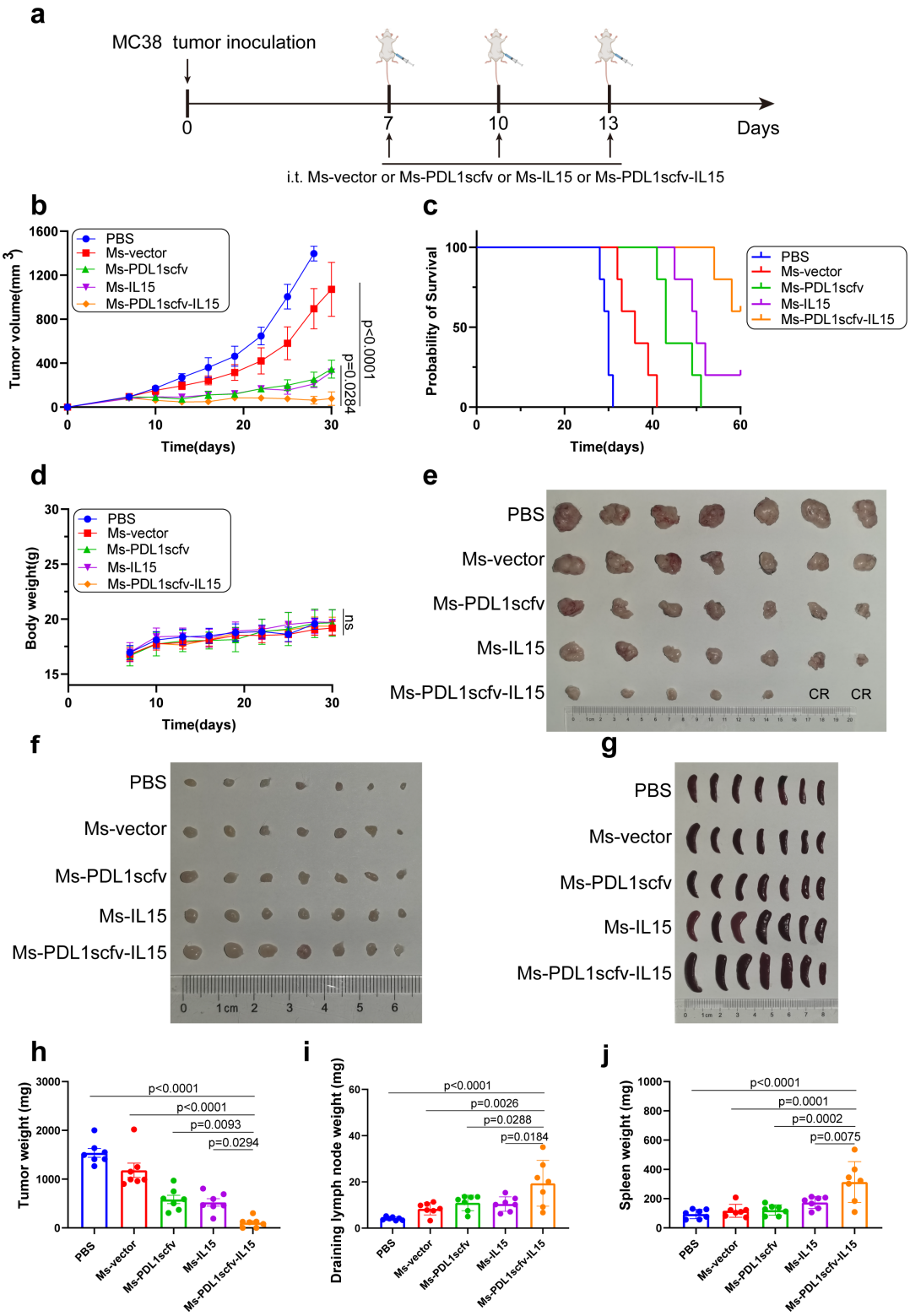

Figure 4 Ms-PDL1scfv-IL15 enhanced antitumor activities against primary tumors. (a) Schematic diagram of the treatment in MC38 tumor-bearing mice. (b–d) C57BL/6 mice were subcutaneously inoculated with MC38 cells. When tumor sizes reached ~100 mm^3, the mice were intratumorally injected with 100 µL of Ms-vector, Ms-PDL1scfv, Ms-IL15, Ms-PDL1scfv-IL15 (1×10^8 CFU per tumor) or PBS on days 7, 10, and 13. (b) Caliper measurement of MC38 tumor were performed on the indicated days (n=7). The error bars represented mean±SEM. P values were calculated by two-way ANOVA and Tukey post-test and correction. (c) Survival curves of MC38 tumor mice in different groups for 60 days (n=5). (d) Average weight of different groups for 30 days (n=5). The error bars represented mean±SEM, p values were calculated by two-tailed unpaired Student's t-tests, ns, not significant. (e–g) On day 7 of the last treatment, the tumor-growing mice were sacrificed, and the tumor masses (e), TDLNs (f), and spleens (g) were photographed and (h–j) weighed (n=7). ANOVA, analysis of variance; CR, complete response; CFU, colony-forming unit; i.t., intratumoral; PBS, phosphate-buffered saline; TDLN, tumor-draining lymph nodes.

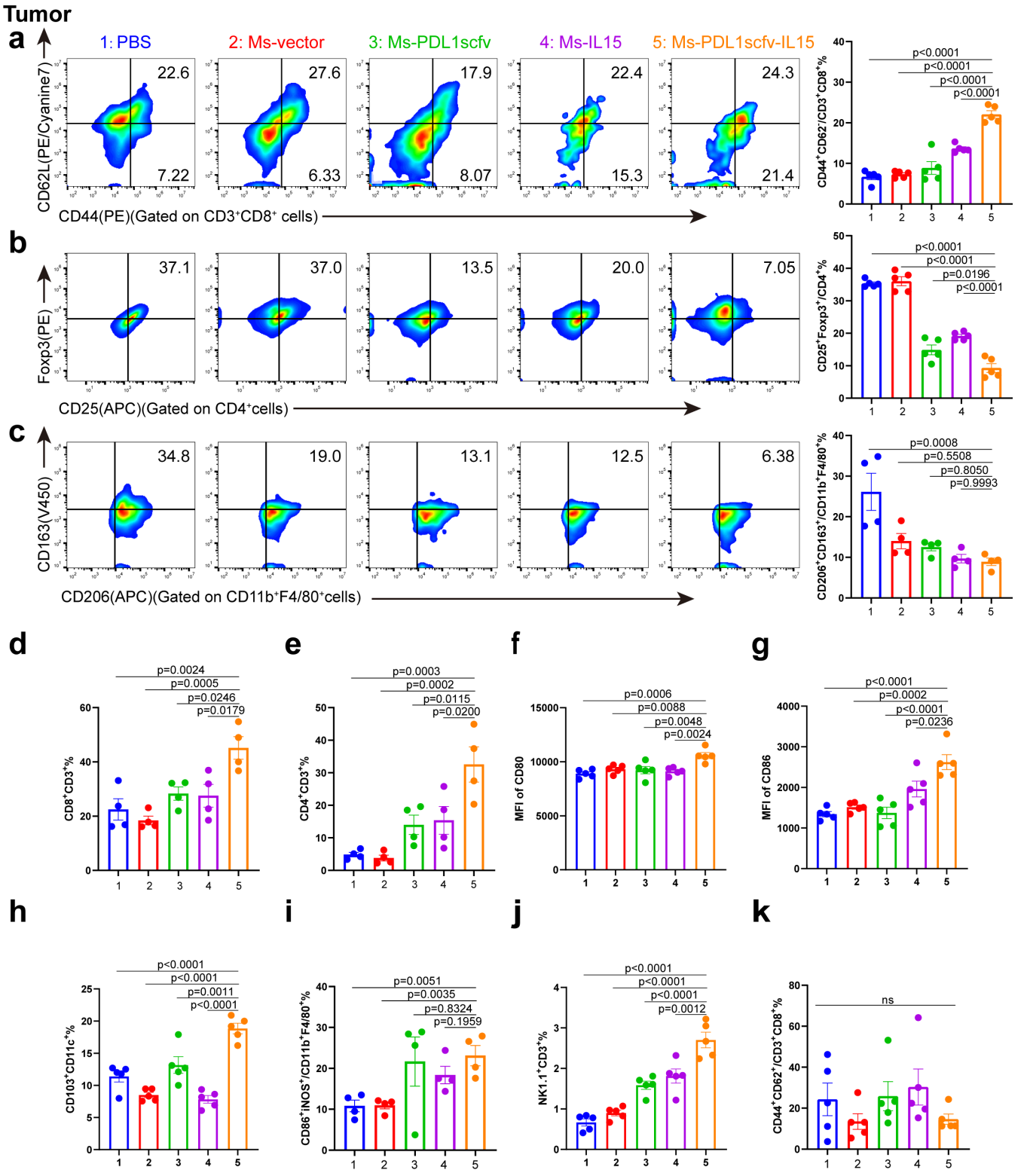

Figure 5 Ms-PDL1scfv-IL15 enhanced tumor infiltration and reprogrammed the immune microenvironment. MC38 tumor-bearing mice in different groups were sacrificed on day 7 of the last treatment. MC38 local tumors were harvested, and digested for preparation of single-cell suspensions, and the proportions of immune cells were analyzed by flow cytometry (n=5). (a–c) Representative flow plots of memory T cells (a, gate on $CD3^+$ $CD8^+$ T cells), $CD4^+$ $CD25^+$ $Foxp3^+$ Tregs (b) and M2 macrophages (c, gate on $CD206^+$ $CD163^+/CD11b^+$ $F4/80^+$ cells). (d, e) The percentage of $CD3^+$ $CD8^+$ T cells (d), $CD3^+$ $CD4^+$ T cells (e) in the tumor microenvironment (n=5). (f, g) Mean fluorescence intensity values of CD80 (f) and CD86 (g). (h–k) The percentage of $CD11c^+$ $CD103^+$ DCs subpopulation (h), M1 macrophages (i, gate on $CD86^+$ $iNOS^+/CD11b^+$ $F4/80^+$ cells), NK cells (j), and the central memory T cells (k, gate on $CD44^+$ $CD62^+/CD3^+$ $CD8^+$ T cells) in tumors (n=5). Data were the mean±SEM, and statistical significance was determined by analysis of two-tailed unpaired Student's t-tests. DCs, dendritic cells; MFI, mean fluorescence intensity; NK, natural killer; PBS, phosphate-buffered saline.

We also examined the immune cells in the TDLN and spleen, both of which are important immune organs. In TDLN, similar to tumor tissue, the Ms-PDL1scfv-IL15 group shows significantly higher MFIs compared with PBS group ($p<0.0001$), supporting enhanced DC maturation (online supplemental figure 8g,h), and the proportion of functional $CD11c^+CD103^+$ DCs also increased to 15.36% (online supplemental figure 8i). In addition, the Ms-PDL1scfv-IL15 group resulted in a significant increase in activated and proliferating $CD8^+$ and $CD4^+$ T cells (online supplemental figure 8d,e). The proportion of NK cells in the Ms-PDL1scfv-IL15 group was eightfold greater than that in the PBS group (online supplemental figure 8f). In the spleen, we mainly examined the changes of T cells, which showed a similar trend as that in tumor tissues. The proportion of Tem in the Ms-PDL1scfv-IL15 group was significantly increased compared with other groups (online supplemental figure 8a), but there was no difference in the proportion of Tcm (online supplemental figure 8c), and the proportion of Tregs was also significantly decreased (online supplemental figure 8b). These results illustrated that Ms-PDL1scfv-IL15 could induce innate and adaptive immune cell activation within the tumor, specifically stimulating tumor-infiltrating $CD8^+$ T cells, DCs and NK cells, inducing M1 polarization of macrophages and reducing Tregs, resulting in enhanced antitumor efficacy.

To further confirm the importance of T cells in Ms-PDL1scfv-IL15 triggered antitumor immune responses, depletion experiments of T cells were performed using anti-CD8 and anti-CD4 antibodies (online supplemental figure 9a), respectively. Notably, the depletion of $CD8^+$ T cells resulted in tumor growth similar to that observed in the PBS group. In the depletion of $CD4^+$ T cells group, although strong enough to delay tumor growth, the observed antitumor effects were far from comparable to those achieved in the Ms-PDL1scfv-IL15 group (online supplemental figure 9b,c). Moreover, we treated tumor-bearing immunodeficient nude mice lacking T lymphocytes with engineered bacteria and found that the tumor inhibition effect of Ms-PDL1scfv-IL15 appeared to be much weakened (online supplemental figure 9d–f). Overall, this further confirms the indispensable role of T cells while other immune cell subsets such as macrophages and NK cells played lesser roles in tumor rejection.

Ms-PDL1scfv-IL15 generates a systemic antitumor and a long-term specific immunological memory response

To assess whether this local efficacy triggers a systemic antitumor immune effect, we first assessed the ability of individual tumor treatments to produce a systemic response to the slow growth of untreated distant tumors, termed an "abscopal effect".[38] To obtain visual effects, we used a luciferase-labeled MC38 (MC38-Luc) colorectal cancer model in which untreated distant tumors were delayed for inoculation by 3 days (figure 6a). We observed that treatment with the Ms-PDL1scfv-IL15 in one tumor led to slower tumor growth in distant untreated tumors compared with other groups (figure 6b–d). In the Ms-PDL1scfv-IL15 group, 40% (2/5) of mice achieved CR and the individual tumor treatments displayed the best tumor control with 80% (4/5) CR. Simultaneous and effective suppression of tumors at both sites resulted in prolonged survival with 80% (4/5) of mice surviving for 60 days in the Ms-PDL1scfv-IL15 group (figure 6e). This may be due to $CD8^+$ T cells, locally activated within treated tumors, circulating systemically to provide therapeutic benefit within untreated tumors sharing a similar antigenic profile.

To further confirm that Ms-PDL1scfv-IL15 could provide long-term protection, we rechallenged CR mice that survived for 60 days by inoculating them with MC38 cells again (figure 6f). The results showed that the tumor inhibition rate of the rechallenge group was 100%, while the tumors of mice in the PBS group grew rapidly (figure 6g,h). Tem is a major source of effector cytokines such as IL-2, IFN-γ, and TNF-α after antigen stimulation. We found that the percentage of Tem ($CD3^+$ $CD8^+$ $CD44^+$ $CD62L^-$) was much higher in the Ms-PDL1scfv-IL15 group (35.30%) than that in the PBS group (5.69%) by isolating spleens for memory T cell analysis (figure 6i,j). Furthermore, the isolated lymphocytes were co-cultured with MC38 cells or B16F10 cells for 24 hours in vitro to detect the tumor cell mortality rate. Only lymphocytes from rechallenge mice co-cultured with MC38 exhibited massive tumor cell death and floated at different E:T under bright-field microscope (online supplemental figure 10a). When the E:T ratio was 5:1, the tumor cell mortality rate increased nearly twofold, and further increased with increasing effector-target ratio, indicating that Ms-PDL1scfv-IL15 make lymphocytes more cytotoxic to kill cancer cells directly (figure 6k, online supplemental figure 10b). In addition, we were surprised to find that lymphocytes from the rechallenge group could kill MC38 cells but not B16F10 cells (figure 6k), suggesting that we induced a specific immune response after Ms-PDL1scfv-IL15 treatment.

Ms-PDL1scfv-IL15 captures neoantigens and activates the NOD-like receptor signaling pathway to generate specific immune responses

To further explore the molecular mechanisms underlying Ms-PDL1scfv-IL15 which induce long-term and specific antitumor protection, we performed bioinformatics analysis of messenger RNA (mRNA) transcriptomes towards Ms-PDL1scfv-IL15 treated tumor. We analyzed the data and found that there were 656 differentially expressed genes (DEGs), with 597 significantly upregulated and 59 downregulated, in PBS versus Ms-PDL1scfv-IL15 (adjusted twofold, p value<0.05) (figure 7a). The Gene Ontology (GO) and Kyoto Encyclopedia of Genes and Genomes (KEGG) functional enrichment analyses identified significantly enriched pathways in DEGs, including inflammatory response, innate immune response, adaptive immune response, pattern recognition receptor activity, NK cell-mediated cytotoxicity and nucleotide-binding

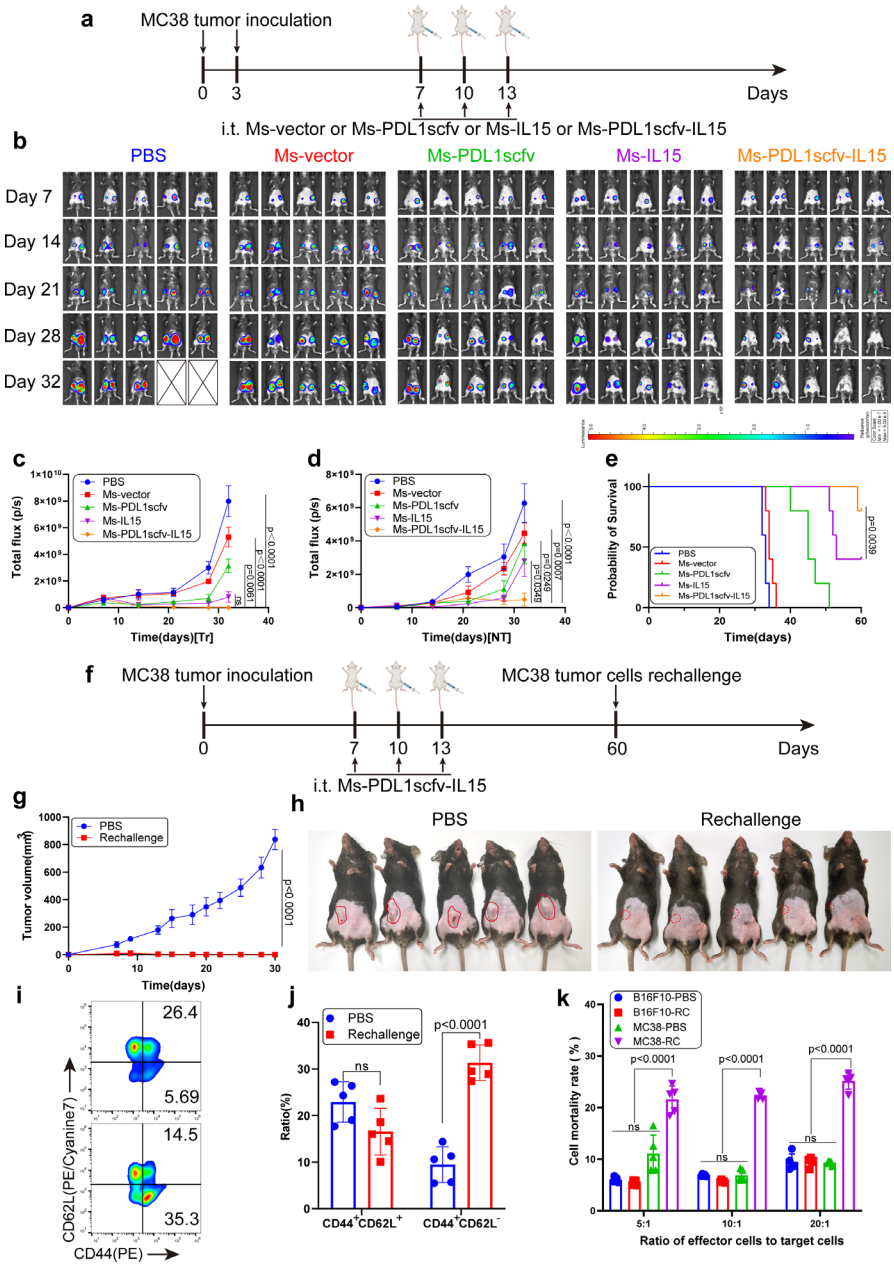

Figure 6 Ms-PDL1scfv-IL15 enhanced antitumor activities against untreated tumors and generated a long-term specific immunological memory response. (a) Schematic diagram of the treatment in MC38-Luc tumor-bearing mice. C57BL/6 mice were subcutaneously implanted with MC38-Luc cells (2×10^6/per) on the left lower sides of the abdomen on day 0, the same procedure was performed 3 days later on the right lower sides of the abdomen, and then mice received treatments on days 7, 10 and 13. (b) Bioluminescence monitoring images of tumor burden on days 7, 14, 21, 28, and 32 after tumor inoculation. (c–e) Total radiant efficiency of signal in treated (Tr) tumors (c) and untreated (NT) tumors (d) in vivo, and survival curve (e) of tumor-bearing mice. Data were the mean±SEM. P values were determined by two-way ANOVA with Tukey's multiple comparisons test. Differences in survival were determined by using the Kaplan-Meier method, and the p value was determined via the log-rank (Mantel-Cox) test. (f) Schematic illustration of evaluating the immune memory effect. Mice cured of MC38 tumor were rechallenged subcutaneously 60 days later with 1×10^6 tumor cells. (g) Tumor growth curves of MC38 rechallenge mice (n=5). (h) Pictures of representative mice were taken 25 days after rechallenge, and the tumors were circled with solid red coils, and the tumors that did not grow were circled with dashed red lines (n=5). (i) Spleens from the rechallenge mice that were photographed above were isolated and ground into single-cell suspensions, and the proportions of memory T (gate on $CD3^+$ $CD8^+$ T cells) cells were analyzed by flow cytometry. Upper panel: memory T cells of PBS group. Lower panel: memory T cells of rechallenge group. (j) The percentage of the effector memory T cells and the central memory T cells in PBS and rechallenge group (n=5). (k) Splenocytes of mice in the PBS or rechallenge group were incubated with CFSE-labeled MC38 or B16F10 cells at effector-to-target ratio of 5:1, 10:1, and 20:1. PI was added 24 hours after incubation and the percentage of dead cells was analyzed by flow cytometry (n=5). Data were the mean±SEM. P values were determined by two-tailed unpaired Student's t-tests. ANOVA, analysis of variance; CFSE, carboxyfluorescein diacetate succinimidyl ester; i.t., intratumoral; PBS, phosphate-buffered saline; PI, propidium iodide.

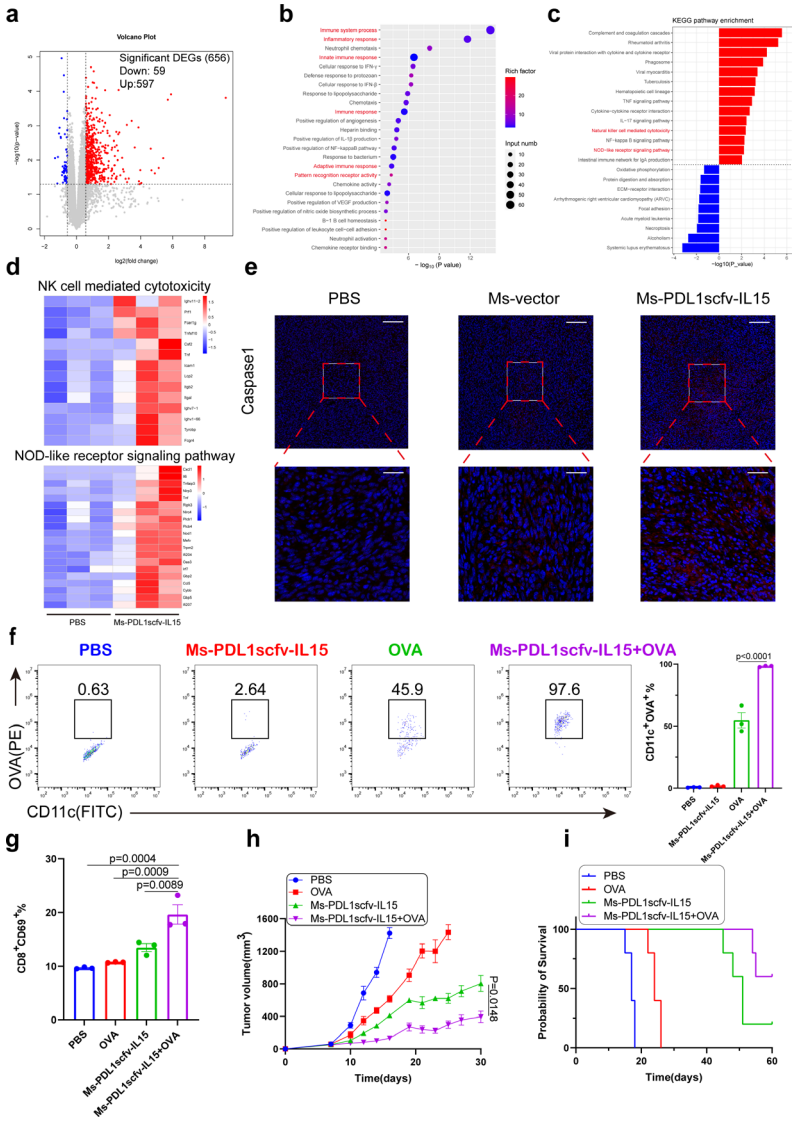

Figure 7 RNA sequencing analysis of Ms-PDL1scfv-IL15 treatment elicits an antigen-specific therapeutic effect. (a) Volcano plot representation of differentially expressed genes (DEGs) between PBS and Ms-PDL1scfv-IL15 group (n=3, adjusted twofold, p values<0.05). The red dots represented significantly upregulated genes, while the blue dots represented significantly downregulated genes. (b) Gene Ontology (GO) analysis of upregulated genes. The enriched GO data were screened, and p values<0.05 were used as the criterion. Term: Functional description in the GO database. Input numb: The number of genes enriched to the term in the input list of differential genes. Rich factor: Enriches the factor. The horizontal axis represents the significance of enrichment (denoted by –log10 (p value), with higher enrichment being more significant), and the vertical axis represents the GO terms of enrichment. Dot size indicates the number of differentially expressed genes included in the GO terms, and dot depth indicates the degree of rich factor enrichment. (c) Kyoto Encyclopedia of Genes and Genomes (KEGG) pathway enrichment of up genes and down genes. (d) Heatmap of differential genes associated with NK cell-mediated cytotoxicity or NOD-like receptor signaling pathway, and the heatmap represents Log 2 fold change values. (e) Immunofluorescence analysis of Caspase1 expression in MC38 treated tumors 7 days after treatments (n=3). Caspase1, red; nucleus, blue. White scale bars: up, 100 µm; down, 20 µm. (f) The percentage of $CD11c^+$ OVA^+ DCs after incubating Ms-PDL1scfv-IL15 with OVA peptide, mDCs and T cells in vitro for 24 hours. Left, representative flow cytometry images. Right, the flow cytometric analysis (n=3). (g) The percentage of CD8+CD69+ T cells after incubating Ms-PDL1scfv-IL15 with OVA peptide, mDCs and T cells in vitro for 24 hours (n=3). Data were the mean±SEM. P values were determined by two-tailed unpaired Student's t-tests. (h, i) C57BL/6 mice were subcutaneously inoculated with OVA-expressing B16F10 cells. When tumor sizes reached~100 mm^3, the mice were intratumorally injected with 100 µL of Ms-PDL1scfv-IL15 (1×10^8 CFU per tumor), OVA peptide (200 µg/mL), PBS or Ms-PDL1scfv-IL15 capturing OVA on days 7, 10, and 13. (h) Caliper measurement of B16F10 tumor were performed on the indicated days (n=5). The error bars represented mean±SEM. P values were calculated by two-way ANOVA and Tukey post-test and correction. (i) Survival curves of B16F10tumor mice in different groups (n=5). ANOVA, analysis of variance; DCs, dendritic cells; ECM, extracellular matrix; FITC, fluorescein isothiocyanate; IL, interleukin; IFN, interferon; mDCs, mature DCs; NK, natural killer; NF-kappa B, nuclear factor kappa-B; NOD, nucleotide-binding oligomerization domain; OVA, ovalbumin; PBS, phosphate-buffered saline; PE, phycoerythrin; TNF, tumor necrosis factor; VEGF, vascular endothelial growth factor.

oligomerization domain (NOD)-like receptor signaling pathway (figure 7b–d), which were related to the activation of both innate and adaptive immune responses. NOD-like receptor (NLR) signaling pathway has been reported as an important immune defense mechanism in organisms, they mediate immune responses by recognizing pathogens and endogenous cellular stress signals through pattern recognition receptors. As shown in the gene heatmap (figure 7d), most of the genes, especially NOD1, NLRP3, IL-6, etc, exhibited enhanced expression after Ms-PDL1scfv-IL15 treatment. Activated NOD1 and NLRP3 inflammasomes further cause the cleavage and activation of pro-Caspase-1, which subsequently promote IL-1β processing and secretion, inducing an inflammatory form of cell death known as pyroptosis. We also verified the programmed cell death of tumor cells via Caspase-1 immunofluorescence (figure 7e).

Furthermore, we wondered whether *M. smegmatis* played a more important role in the whole antitumor immune process, especially in the specific immune response. *M. smegmatis* has been reported to be rapidly destroyed by phagolysosomal proteases in the phagosome of infected cells, which may facilitate better release of therapeutic agents or better cross-presentation of foreign antigens to T cells.[28 29] We hypothesized that Ms-PDL1scfv-IL15 could potentially capture antigens during tumor regression, which were then phagocytosed by DCs and presented to T cells, triggering a specific immune response. We tested the hypothesis by immunofluorescence co-localization using fluorescently FAM-labeled ovalbumin (OVA) antigen peptide incubated with Dil-labeled Ms-PDL1scfv-IL15 for 2 hours in vitro, and the results showed that the OVA peptide was effectively captured by Ms-PDL1scfv-IL15 and adhered to the bacterial surface (online supplemental figure 11). Furthermore, after incubating OVA peptide adsorbed by Ms-PDL1scfv-IL15 with mature DC and T cells in vitro for 24 hours, the proportion of OVA-bound DCs on the cell surface was detected by flow cytometry. We found that there were only 54.8% DCs in the OVA group and 98.2% in the Ms-PDL1scfv-IL15+OVA group (figure 7f). We also detected the activation of T cells. Compared with the PBS group, the proportion of $CD8^+CD69^+$ cells in the Ms-PDL1scfv-IL15+OVA group increased more than twofold (figure 7g, online supplemental figure 12a). Next, OVA-expressing B16F10 melanoma mouse models were used to explore the initiation of tumor-specific immune responses. Ms-PDL1scfv-IL15+OVA group showed superior antitumor effect and significantly prolonged the survival time of mice (figure 7h,i, online supplemental figure 12b,c). In brief, our results revealed that Ms-PDL1scfv-IL15 could capture the debris or antigens after tumor cell apoptosis, and effectively present them to T cells (especially $CD8^+$T cells) through DCs to induce the activation and proliferation of T cells and generate specific immune responses.

Ms-PDL1scfv-IL15 as a robust multipotent therapy platform

To assess the broad applicability, we tested Ms-PDL1scfv-IL15 in a less immunogenic B16F10 melanoma model.[39] We performed intratumoral injection of the Ms-PDL1scfv-IL15 in subcutaneous B16F10 tumors and observed a significant therapeutic benefit and prolonged survival (figure 8a–d). We further analyzed the immune cells in the tumor microenvironment (TME) and found that DCs (23.82%) were effectively induced to mature by Ms-PDL1scfv-IL15 (figure 8e), and the infiltration of $CD3^+CD8^+$ T cells in the tumor tissue was increased. The proportion of Tem and Tcm (figure 8f, online supplemental figure 13f) was also significantly increased (35.92% and 19.45%, respectively). Macrophages were also polarized, compared with the PBS group (M2 ratio was 38.82%, M1 ratio was 14.16%), with the M2 ratio of Ms-PDL1scfv-IL15 decreasing to 12.21%, and M1 ratio increasing to 67.98% (figure 8g, online supplemental figure 13e). In the TDLN and spleen, the proportion of mature DCs and Tem also changed significantly, we observed a significant increase in the proportion of mature DCs (24.94% in TDLN, 19.00% in spleen) and Tem (13.48% in TDLN, 34.04% in spleen) in the Ms-PDL1scfv-IL15 group (online supplemental figure 13a,b,g and online supplemental figure 13c,d,h). These results demonstrated the power of the Ms-PDL1scfv-IL15 to successfully convert the “cold” tumors to “hot” tumors, thus exerting a robust antitumor effect. To further verify the universality of our treatment platform, we tested the therapeutic effect of Ms-PDL1scfv-IL15 in CT26 colorectal cancer and 4T1 breast cancer, which are less immunogenic and more malignant.[40 41] As shown in online supplemental figure 14, we observed that in both tumor models, the intratumoral injection of Ms-PDL1scfv-IL15 resulted in significant ($p<0.0001$) therapeutic benefit and prolonged survival, while there was no significant difference in body weight among the mice in the different groups. Unexpectedly, we found that Ms-PDL1scfv-IL15 was also effective in inhibiting tumor metastasis, and the number of lung tumors in the 4T1 tumor model was significantly reduced. The above results suggested that increased lymphocyte activation and modulation of the TME are more amenable to treatment.

To expand on this therapy platform, we sought to explore combinatorial treatments to enhance antitumor activity in the MC38 tumor model. Motivated by recent literature exploring the use of GM-CSF as a cancer therapy, we hypothesized that GM-CSF could enhance the function of DCs and promote the differentiation and activation of monocytes/M1 macrophages, indirectly recruit T cells into the TME through enhanced antigen presentation, and ultimately cooperate with Ms-PDL1scfv-IL15 produced checkpoint inhibitors and cytokines.[42–44] Ms-PDL1scfv-IL15-treated mice received GM-CSF (i.t.) three times, as illustrated in figure 8h. and we observed an enhanced antitumor effect when compared with the monotherapies, with greater survival benefit (figure 8i,k, online supplemental figure 15). The improved therapeutic

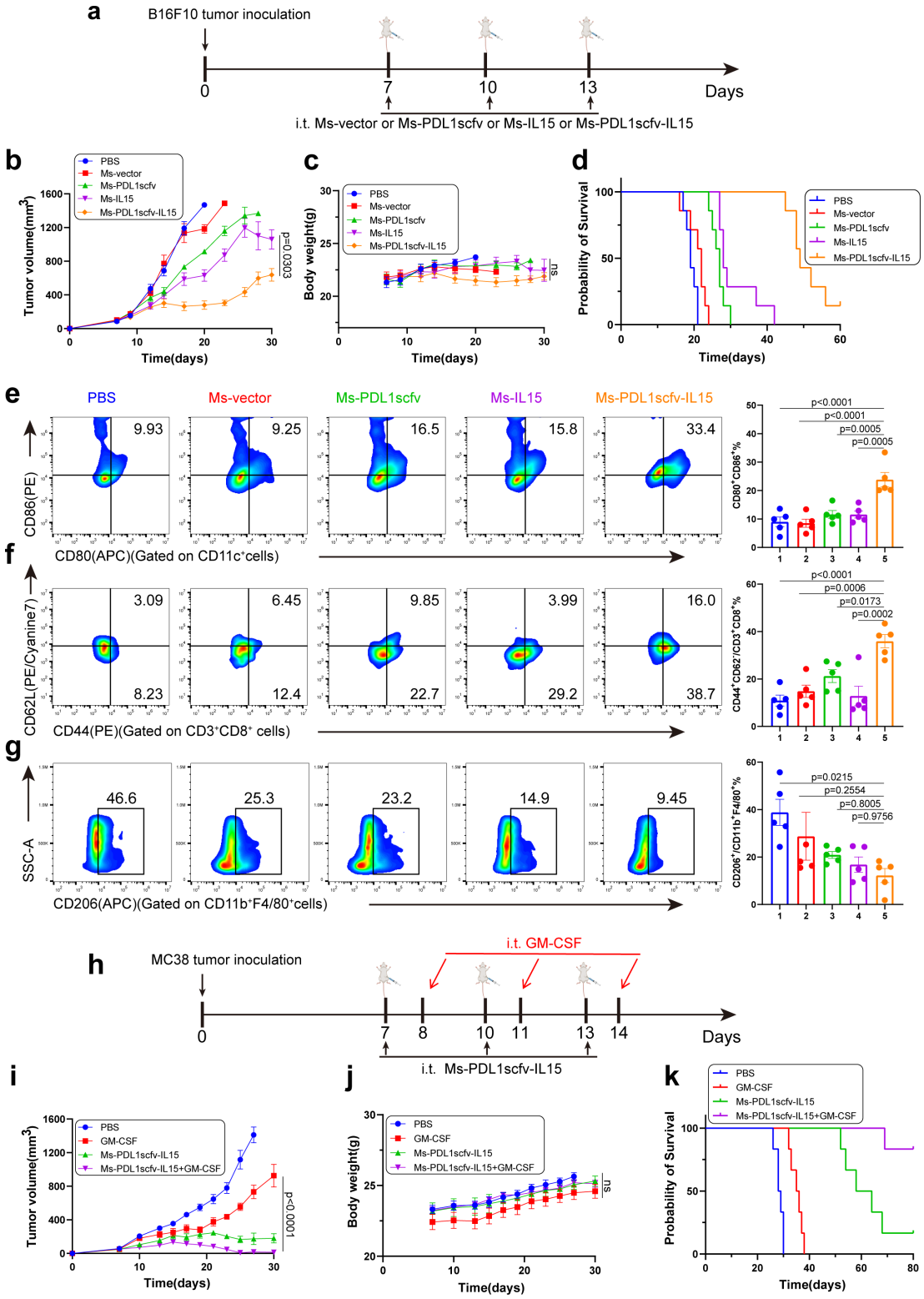

Figure 8 The Ms-PDL1scfv-IL15 platform allows multiple therapeutics to be effectively combined for an enhanced antitumor effect in poorly immunogenic cancers. (a) Schematic diagram of the treatment in B16F10 tumor-bearing mice. (b–d) B16F10 tumor volume (b), average weight (c), and survival curves (d) were monitored using the same treatment schedule as in figure 4b–d. (e–g) The percentage of $CD11c^+$ $CD80^+$ $CD86^+$ mDCs (e), memory T cells (f, gate on $CD3^+$ $CD8^+$ T cells), and M2 macrophages (g) in the tumor microenvironment (n=5). Left, representative flow cytometry images. Right, the flow cytometric analysis (n=5). Data were the mean±SEM, and statistical significance was determined by analysis of two-tailed unpaired Student's t-tests. (h) Schematic diagram of administration route for Ms-PDL1scfv-IL15 combined with GM-CSF in tumor suppression experiment. MC38 tumor volume (i), average weight (j), and survival curves (k) were monitored in each group. APC, allophycocyanin; mDCs, mature dendritic cells; GM-CSF, granulocyte-macrophage colony-stimulating factor; i.t., intratumoral; PBS, phosphate-buffered saline; PE, phycoerythrin; SSC-A, side scatter-area.

outcome suggested a useful combination therapy that is well tolerated by mice, as was evidenced by the maintenance of health and body weight (figure 8j). We further examined the immune cell phenotypes in tumor tissues. The results demonstrated that in the Ms-PDL1scfv-IL15 combined with GM-CSF treatment group, the MFI of CD80 and CD86 (online supplemental figure 16a,b) was significantly elevated ($p<0.001$), and the proportion of CD103-positive cell subsets increased by 1.7-fold compared with the control group (online supplemental figure 16c). Additionally, this treatment group exhibited an increased proportion of M1-type macrophage phenotypes and a marked reduction in M2-type macrophage phenotypes (online supplemental figure 16d,e). These experimental results demonstrate that GM-CSF and Ms-PDL1scfv-IL15 exhibit a synergistic effect, which enhances DCs functional activity and promotes macrophage polarization toward the pro-inflammatory, antitumor M1 phenotype. The combination of Ms-PDL1scfv-IL15 and GM-CSF has potential clinical application value.

Biosafety evaluation of Ms-PDL1scfv-IL15

Intratumoral injection of bacteria may have potential biosafety implications although no significant differences in body weight were observed across mouse models. At the endpoint, the in vivo toxicity of Ms-PDL1scfv-IL15 was investigated by measuring the levels of serum aspartate transaminase (AST), alanine transaminase (ALT), alkaline phosphatase (AKP), lactate dehydrogenase (LDH), creatinine (CREA) and urea in each group and we evaluated histological sections of their primary organs. Relative to the healthy control, there were no discernible changes in the H&E-stained heart, liver, spleen, lung, and kidney (online supplemental figure 17a). Furthermore, there were no evident changes in the serum of AST, ALT, AKP, LDH, CREA, and urea levels after treatment with Ms-PDL1scfv-IL15 versus other groups (online supplemental figure 17b), indicating no hepatotoxicity or nephrotoxicity. In immunotherapy, life-threatening side effects such as cytokine storm may occur. Therefore, at the endpoint, we also measured the concentrations of inflammatory factors and chemokines in serum and assessed the systemic inflammatory response of Ms-PDL1scfv-IL15. Overall, the serum concentrations of IFN-γ, IL-2, IL-13, IL-4, IL-10, IL-5, IL-6, and TNF-α were generally similar among all the groups without a statistical difference (online supplemental figure 17c). Consequently, Ms-PDL1scfv-IL15 presents good biosafety.

DISCUSSION

Here, we have demonstrated a fusion protein of PD-L1 antagonist and IL-15 cytokine expressed and delivered by *M. smegmatis* as an in situ vaccine for tumor therapy, which enabled local therapeutic production and improved antitumor activity in multiple syngeneic mouse models. Moreover, we have characterized that Ms-PDL1scfv-IL15 can effectively block tumor cell escape and activate immune cells, eliciting systemic tumor regressions. Notably, Ms-PDL1scfv-IL15 captures antigen fragments in the tumor microenvironment, which remarkably initiates tumor antigen-specific immune response, leading to durable tumor regression and specific antitumor immunity (online supplemental figure 18).

M. smegmatis was selected on the basis of safety, practicability, and effectiveness compared with some other attenuated strains which might risk toxicity recurrence.[25 27 45 46] Moreover, *M. smegmatis* cannot move freely due to the lack of flagella, which can exert the advantages of local treatment and minimize the risk of systemic toxicities.[47] *BCG* is currently the only live bacterial drug preparation approved by the FDA for the treatment of cancer.[22] *M. smegmatis* has a similar cell wall composition with *BCG*, which is associated with the enhanced efficacy of immunotherapy and is better than *BCG* in inducing macrophages to produce cytokines.[48] In addition, it can activate and induce the maturation of DCs by upregulating major histocompatibility complex class I and costimulatory molecules, which can trigger $CD8^+$T cell-mediated immune responses.[32] In our study, it was found that *M. smegmatis* could capture free antigen fragments and boost DCs cross-presenting them to T cells to induce T cell-specific immune killing, which provided long-term antitumor protection. However, we did not investigate how Ms-PDL1scfv-IL15 captured the peptide in detail. We hypothesized that the possible mechanisms are as follows: one was that negatively charged bacteria could bind to the positively charged groups in the peptide[49]; the other was that *M. smegmatis* is hydrophobic due to the peptidoglycan on its surface, which is prone to polymerize with hydrophobic antigenic peptides.[50]

Regarding the translational potential of Ms-PDL1scfv-IL15, we have shown that Ms-PDL1scfv-IL15 delivered intratumorally results in tumor regression in multiple different tumor models. Ms-PDL1scfv-IL15 promotes the maturation of DCs, improves their antigen-presenting capacity, activates and proliferates T and NK cells, inhibits Tregs in TME, enhances the ability of immune cells to infiltrate tumors, and induces M1 macrophage polarization. As a potent immune adjuvant,[25] Ms-PDL1scfv-IL15 also significantly sensitized “cold” tumors to “hot” tumors in our study. Moreover, we have demonstrated an abscopal effect, providing a potential strategy for the treatment of metastatic lesions if a primary tumor site is inaccessible for injection. These elements are advantageous in a clinical setting, where minimally invasive and self-sustained therapies are more desirable.

Some limitations still existed in our study. Several tumor-bearing mice might relapse 1 month after the treatment especially in “cold” tumor models. It is necessary to investigate this phenomenon from a molecular perspective and provide some more effective strategies such as adjusting the frequency and dose of administration and combining Ms-PDL1scfv-IL15 with other effective immunotherapies. In addition, our current study did not explore the mechanism by which the bacterial lysates are cleared from the

body. Moreover, it might be worthwhile to further study the changes of immune cells in nontreated tumors. If necessary, single-cell transcriptomics may be performed to analyze differences at the genetic level, thoroughly uncovering the development and metabolism of tumors. Finally, to make this therapeutic platform more clinically relevant, alternative routes of therapeutic administration need to be considered in more translational animal models.

In summary, we have built a stable engineered Ms-PDL1scfv-IL15 therapeutic platform as an in situ vaccine, which provided a durable delivery vehicle. In the platform, therapeutic production is sustained and toxicities are minimized, which can provoke robust innate and tumor-specific adaptive immune responses in a broader range of cancer patients.

MATERIALS AND METHODS

Bacterial strains, cell lines

M. smegmatis, Escherichia coli B21, pET-30a, and pMV261 vector were stored in our laboratory. *M. smegmatis* was grown in Middlebrook 7H9 broth containing 10% OADCm, 0.2% (v/v) glycerol, 0.05% (v/v) Tween 80. *E. coli* strains were incubated in Luria-Bertani medium at 37°C with shaking at 220 rpm. Enumeration of mycobacterial colony-forming units was performed by plating onto mycobacteria 7H10 agar containing 0.2% (v/v) glycerol. *M. smegmatis* were washed twice in PBS and stored frozen at −80°C in 25% sterile glycerol/PBS. MC38, B16F10, A375, 4T1, and CT26 cells were obtained from the Cell Bank of Shanghai Institute of Biochemistry and Cell Biology. All the cells were maintained in Roswell Park Memorial Institute (RPMI) 1640 (Gibco) supplemented with 10% fetal bovine serum, 100 U/mL penicillin, and 100 µg/mL streptomycins at a humidified 37°C, 5% CO_2 incubator. MC38-Luc cells were generated by luciferase lentivirus (GeneChem, Shanghai, China) transfection.

Animal models

The experimental protocols require animals to be euthanized when the tumor burden reaches 2 cm in diameter or on recommendation by veterinary staff. BALB/c (for 4T1 and CT26 tumors), nude (for MC38 tumors), and C57BL/6 (for MC38 and B16F10 tumors) male/female mice aged 5–6 weeks were purchased from Shanghai Sippr-BK laboratory animal (Shanghai, China) and kept in the specific pathogen-free (SPF) Laboratory Animal Center of Affiliated Nanjing Drum Tower Hospital of Nanjing University Medical School.

MC38, B16F10, 4T1, and CT26 cells were washed three times in PBS and resuspended at 2×10^7, 5×10^6, 1×10^7, and 1×10^7 cells/mL in PBS, respectively, and 100 µL of cell suspension was then injected subcutaneously into each hind flank. The tumor volume was determined by caliper measurements (length×width^2×0.5), and mice were randomly assigned to treatment groups after tumor volume reached approximately 100 mm^3. In the abscopal effect mouse model, MC38-Luc cells were washed in PBS and resuspended at 2×10^7 cells/mL in PBS, and 100 µL of cell suspension was then injected subcutaneously into both hind flanks. The untreated distant tumors were delayed for inoculation by 3 days. In the rechallenge mouse model, MC38 cells were injected at a concentration of 1×10^7 cells/mL in PBS. In the metastatic tumors mouse model, 4T1 cells were prepared as above and injected via the tail vein at a concentration of 5×10^6 cells/mL in PBS, with a total volume of 100 µL injected per mouse. For treatment with bacteria, bacteria were cultured in a 37°C shaking incubator to reach the stationary phase of growth in 7H9 broth with appropriate Kanamycin antibiotics. When the bacteria reached the logarithmic growth phase, bacteria were harvested and washed three times with PBS, and then resuspended in ice-cold PBS. Intratumoral injections were performed every 3 days for a total of three treatments.

Preparation of engineered bacteria

The binding antibody moieties of fusion protein are VH–(Gly4Ser)3-VL scfv derived from monoclonal antibodies, αPD-L1, avelumab (PDB:5GRJ_H, PDB:5GRJ_L), the binding cytokine moieties of fusion protein are IL-15 and IL-15Rα sushi-domain from reported previously (online supplemental table 1).[31] *BCG* and *M. smegmatis* α-antigen signal sequence derived from UniProt database. The complementary DNA was cloned into the *E. coli*-mycobacterial shuttle vector pMV261 plasmid under the control of the constitutively expressed mycobacterial heat shock protein promoter 60 (Hsp60). Plasmids were introduced into mycobacteria by electroporation at 4°C for *M. smegmatis*. Standard conditions of 2.5 kV, 25 µF, and 1,000 Ω were employed and a 2 mm cuvette was used (Bio-Rad, Richmond, California, USA). Clones were selected based on resistance to kanamycin (50 µg/mL). PDL1scfv-IL15 protein was expressed in *E. coli* BL21 and purified by nickel column, which was treated according to IL-15 concentration of 1×10^8 CFU bacteria. Lysates of Ms-PDL1scfv-IL15 were obtained by ultrasonication and then treated at an equivalent volume of 1×10^8 CFU bacteria per mouse. Ms-PDL1scfv-IL15 was inactivated by paraformaldehyde and then treated with 1×10^8 CFU bacteria per mouse.

Western blot

When engineered bacteria were cultured to reach the stationary phase of growth in 7H9 broth, bacteria were harvested and clarified by centrifugation at 10,000×g for 10 min, and the supernatant of the culture medium was concentrated by freeze drying to obtain secreted proteins. The bacteria were washed twice with PBS+0.02% Tween 20 (PBST), resuspended in 1 mL PBST, sonicated, and centrifuged at 10,000×g for 15 min. The supernatant of cytoplasmic proteins was collected, and the precipitate was resuspended in 1 mL PBS. Each protein sample was separated by 12% sodium dodecyl sulfate-polyacrylamide gel electrophoresis (SDS-PAGE), then electrotransferred

to polyvinylidene fluoride (PVDF) membrane and blocked with 5% skim milk powder at room temperature for 1–2 hours. After being washed three times with PBST, FLAG monoclonal antibody (Abcam, ab236777) or human IL-15 monoclonal antibody (Abcam, ab134177) was added with a 1:1,000 dilution, and the reaction was performed at room temperature for 2 hours. After washing with PBST three times, horseradish peroxidase (HRP)-labeled goat anti-mouse IgG or HRP-labeled goat anti-rabbit IgG (Beyotime, Shanghai, China) was added with a 1: 1,000 dilution and incubated at room temperature for 1 hour. PBST was washed three times and ECL Western blotting Substrate (Tanon, Shanghai, China) was used for color development.

Characterization of Ms-PDL1scfv-IL15

When the bacteria reached the logarithmic growth phase, the secreted proteins and bacteria were collected by freeze drying and centrifugation. To investigate the binding of PD-L1scfv, 1×10^6 A375 or MC38 cells were co-incubated in a 96-well bottom plate with a constant concentration of the mixture described above. Samples were incubated at room temperature for 2 hours, washed with ice-cold PBS, and then co-incubated with the fluorescently-conjugated anti-FLAG mAb (L5, BioLegend) or anti-PD-L1 mAb (MIH7, BioLegend) at room temperature for 30 min, cells were analyzed using BD Accuri C6 (BD Bioscience, USA) and analyzed by FlowJo software. To investigate the activation of IL-15, T cells were isolated from C57BL/6 mouse spleen or human peripheral blood mononuclear cells (PBMC), and then cells were labeled with CFSE at a final concentration of 2 µM in PBS to 5×10^6 cells/mL, and 100 µL per well was added with a constant concentration of engineered bacteria to a 96-well plate. Cells were harvested after 5 days for flow assays. In the cell counting kit 8 assay, Ms-PDL1scfv-IL15 was diluted to different concentrations and incubated with T cells. Added penicillin-streptomycin solution to each sample 24 hours prior to measurement for bacteria eradication. After 5 days, all samples were detected according to the kit protocol. The human IL-15 ELISA Pair Set (Sino Biological) was performed using standard methods. Briefly, 96-well ELISA plates were coated by incubating with 1.0 µg/mL of recombinant human IL-15 at 4°C overnight, then washed three times with PBST and blocked with 5% bovine serum albumin for 2 hours at room temperature. After washing the plates, serial dilution samples of MS-PDL1scFv-IL15 were added to the plates in duplicate and incubated at room temperature for 2 hours. Plates were washed three times and incubated with peroxidase affinity pure goat anti-human IgG (H+L) at room temperature for 1 hour. After being washed, 3,3',5,5'-tetramethylbenzidine (TMB) single component substrate solution (Solarbio, Beijing, China) was added to the plates and incubated in the dark for 3–5 min. After terminating the reaction with 2 M sulfuric acid, absorbance was read at 450 nm.

In vitro uptake and stimulation of bacteria by BMDCs

BMDCs were obtained from bone mesenchymal stem cells harvested from C57BL/6 mice freshly. Then the cells were cultured with RPMI 1640 medium containing 10% fetal bovine serum (FBS) and 1% penicillin-streptomycin as described in the previous literature.[51] 20 ng/mL rmGM-CSF (Xiamen Amoytop Biotech, China) and 10 ng/mL rmIL-4 (PeproTech, USA) were added to induce the cells to differentiate into DCs. The medium was replaced every 3 days and these DCs were centrifuged, and collected for use on day 8. Ms-PDL1scfv-IL15 stained by DiO (Bridgen, Beijing, China) were co-incubated with DCs stained by DiI (Bridgen, Beijing, China) and imaged under a confocal laser scanning microscope (Leica, Germany) to assess the process of internalization into DCs.

Effects of different concentrations of Ms-PDL1scfv-IL15 on BMDCs were studied in vitro by co-culture for 24 hours. Then DCs were collected by centrifugation at 500×g for 5 min and incubated with fluorescein isothiocyanate (FITC)-CD11c, allophycocyanin (APC)-CD80, and phycoerythrin (PE)-CD86 for 20 min at room temperature to flow assays.

Activation of T cells by antigenic peptides in vitro

Lymphocytes and DCs were isolated from splenocytes and bone mesenchymal stem cells of C57BL/6 mice. The mature DCs on the 96-well plate were 2×10^5 cells, and the co-culture was carried out according to the ratio of bacteria : T cells : DCs=100:10:1. The OVA peptide was dissolved in 1 mL medium and a final concentration of 20 mg/mL was added to co-culture for 24 hours. Finally, the cells were collected by centrifugation and assessed by flow cytometry analysis of anti-CD8-PE/Cyanine5.5, anti-CD69-FITC, and anti-CD25-APC.

In vivo real-time near-infrared fluorescence imaging

Near-infrared imaging was used to localize Ms-PDL1scfv-IL15 quantitatively. Ms-PDL1scfv-IL15 labeled with DiR (Bridgen, Beijing, China) was injected i.t. Then we used the CRi Maestro In Vivo Imaging System (Cambridge Research & Instrumentation, Massachusetts, USA) to anesthetize and scan the mice at indicated time points post Ms-PDL1scfv-IL15 administration. Tumors, TDLNs, and central organs, including heart, liver, spleen, lung, and kidney were excised and imaged for resected tissue imaging after the mice were sacrificed under deep anesthesia.

Bacterial colonization in vivo

After intratumoral injection of Ms-PDL1scfv-IL15 in the treated tumor, we collected the major organs (heart, liver, spleen, lung, and kidney), blood, TDLN, and tumor tissue at desired time points. Then we weighed and homogenized these samples at 4°C in sterile PBS. The homogenates were serially diluted and spread on 7H10 plates and incubated at 37°C for 3–6 days. Bacterial colonies were counted and computed as CFU/g of tissue.

Plasmid retention rate

The engineered bacteria were serially diluted and spread on a 7H10 solid medium. Subsequently, 100 single colonies were selected and inoculated on both 7H10 solid medium and 7H10 solid medium supplemented with kanamycin and incubated at 37°C for 3–6 days. Finally, the retention rate of the engineered bacteria plasmid was determined by quantifying the number of bacteria present on the kanamycin-containing 7H10 solid medium.

Depletion studies

The depleting antibodies were administered intraperitoneally 2 days prior to the initiation of treatments. For depletion of immune cell subsets, mice were injected with anti-mouse CD8 (clone 2.43, Bio X Cell, 400 µg per injection two times a week), anti-mouse CD4 (clone GK1.5, Bio X Cell, 200 µg per injection weekly).

Histological analysis

To further determine the trajectories of Ms-PDL1scfv-IL15 in vivo, we harvested tumors, TDLNs, and main organs (heart, liver, spleen, lung, and kidney) after intratumoral injection of DiO-labeled Ms-PDL1scfv-IL15 at the required time. After washing with PBS, the frozen sections were mounted with DAPI (Beyotime, Shanghai, China) to visualize nuclei and then imaged on a confocal laser scanning microscopy (Leica, Germany). The last treated tumor was collected and incubated paraformaldehyde-fixed tumor tissue sections with primary antibodies (Abcam) for 2 hours at 37°C and then washed with PBS three times. Image-Pro Plus 6.0 was adopted to analyze each and mean density (integrated optical density per unit area (IOD/area)) was used to analyze protein expression. The organ tissues mentioned above were fixed in formalin, paraffin-embedded, sectioned, and stained with H&E. Slides were scanned on a Zeiss Axioscan.Z1 with a 20×objective and analyzed in ImageJ.

Flow cytometry

Tumor tissues, TDLNs, and spleens were harvested at the indicated time points. Single-cell suspensions of spleens and TDLNs were prepared by the mechanical trituration method. For isolation of tumor-infiltrating lymphocytes, tumor tissues were excised, then minced, and digested in RPMI 1640 with collagenase type IV (1 mg/mL, Sigma) in an incubator for up to 2 hours at 37°C to achieve a single-cell suspension. Once a single-cell suspension was achieved, samples were washed and stained with specific antibodies for 20 min at room temperature in the dark and washed before analysis. LEGENDplex MU Th1/Th2 Panel (8-plex) V03 (BioLegend) was used to detect and analyze the level of cytokines in the tumor cell supernatant or serum. Cells were analyzed using BD Accuri C6 (BD Bioscience, USA) and analyzed by FlowJo software. Antibodies to CD11c (N418, FITC, 117306), CD80 (16–10A1, APC, 104714), CD86 (GL-1, PE, 105008), CD8a (53–6.7, PerCP/Cyanine5.5, 100734), CD103 (2E7, PE, 121406), CD3 (500A2, FITC, 152304), PD1 (29F.1A12, APC, 135210), CD4 (GK1.5, PE, 100408), CD8a (53–6.7, APC, 100712), CD25 (PC61, APC, 102012), CD69 (H1.2F3, PE/Cyanine7, 104512), CD69 (H1.2F3, FITC, 104506), FoxP3 (MF-14, PE, 126404), CD44 (IM7, PE, 103008), CD62L (MEL-14, PE/Cyanine7, 104418), CD11b (M1/70, APC, 101212), F4/80 (BM8, PE/Cyanine5, 123112), CD206 (C068C2, PE, 141706), Fixable Viability (BV510, 423121), CD163 (S15049I, BV421, 155309), iNOS (W16030C, PE, 696806) were purchased from BioLegend. Intracellular staining for FoxP3 was performed using the True-Nuclear Transcription Factor Buffer Set (BioLegend).

RNA sequencing

We rapidly excised the tumor and froze it with liquid nitrogen 7 days after the last treatment. The mRNA samples of the PBS group and Ms-PDL1scfv-IL15 group were used for RNA sequencing (RNA-seq) (SeqHealth Tech, Wuhan, China). Quantification of gene expression and differential expression analysis was performed using the DESeq2 Bioconductor package (online supplemental table 2). Functionally related GO terms for biological processes were analyzed by GOSeq (V.1.34.1), while the KEGG enrichment analysis used the database (http://en.wikipedia.org/wiki/KEGG). GO network analysis of significantly upregulated genes in tumors was analyzed by Cytoscape software. The RNA-seq data has been deposited into the NCBI database (Accession number: GSE280146).

Statistics

Statistical analysis was performed using GraphPad Prism V.9. When passing the normality test, a two-tailed Student's t-test was used to compare the two groups. Otherwise, a Mann-Whitney U test was used. Repeated-measures two-way analysis of variance with Bonferroni's correction was used to compare the effect of multiple levels of two factors with multiple observations at each level (for tumor volumes). Animal survival is presented using Kaplan-Meier survival curves and was statistically analyzed using the log-rank test. The data presented in the figures are mean±SD. P values<0.05 were considered to be statistically significant. For fluorescence-activated cell sorting (FACS) studies and other experiments, Student's t-tests were used. All experiments were repeated at least three times. Flow cytometry data were collected with BD Accuri C6 (BD Bioscience, USA) and analyzed using FlowJo. Figures were designed in Adobe Photoshop.

Acknowledgements This work is authorized and supported by BioRender, and the agreement numbers between the Graphical abstract and figure 1a are GX27EQVW3C and JL27EQX7GV, respectively.

Contributors YM and BL conceived and designed the experiments. YM and JZ performed the experiments. JSha, LL, FL, XS, YY, JShe, and RL assisted in the experiments and data analysis. YM and JZ prepared the manuscript. BL is responsible for the overall content as guarantor.

Funding This work was financially supported by the National Natural Science Foundation of China (grant no. 82272811 to BL) and Jiangsu Province Key Research and Development Program (grant no. BE2023654 to BL).

Competing interests None declared.

Patient consent for publication Not applicable.

Ethics approval The Laboratory Animal Care and Use Committee of the Affiliated Nanjing Drum Tower Hospital of Nanjing University Medical School (20211103) approved the use of mice and all mouse work presented here.

Provenance and peer review Not commissioned; externally peer reviewed.

Data availability statement Data sharing not applicable as no datasets generated and/or analysed for this study.

ORCID iDs
Jie Shao http://orcid.org/0000-0003-1222-0505
Jie Shen http://orcid.org/0000-0003-3157-4640
Baorui Liu http://orcid.org/0000-0002-2539-7732

REFERENCES

1 Zhu J, Ke Y, Liu Q, *et al*. Engineered Lactococcus lactis secreting Flt3L and OX40 ligand for in situ vaccination-based cancer immunotherapy. *Nat Commun* 2022;13:7466.
2 Saxena M, van der Burg SH, Melief CJM, *et al*. Therapeutic cancer vaccines. *Nat Rev Cancer* 2021;21:360–78.
3 Melero I, Castanon E, Alvarez M, *et al*. Intratumoural administration and tumour tissue targeting of cancer immunotherapies. *Nat Rev Clin Oncol* 2021;18:558–76.
4 Lin Z, Meng F, Ma Y, *et al*. *In situ* immunomodulation of tumors with biosynthetic bacteria promote anti-tumor immunity. *Bioact Mater* 2024;32:12–27.
5 Naidoo J, Page DB, Li BT, *et al*. Toxicities of the anti-PD-1 and anti-PD-L1 immune checkpoint antibodies. *Ann Oncol* 2016;27:1362.
6 Baxi S, Yang A, Gennarelli RL, *et al*. Immune-related adverse events for anti-PD-1 and anti-PD-L1 drugs: systematic review and meta-analysis. *BMJ* 2018;360:k793.
7 Patidar M, Yadav N, Dalai SK. Interleukin 15: A key cytokine for immunotherapy. *Cytokine Growth Factor Rev* 2016;31:49–59.
8 Berrien-Elliott MM, Becker-Hapak M, Cashen AF, *et al*. Systemic IL-15 promotes allogeneic cell rejection in patients treated with natural killer cell adoptive therapy. *Blood* 2022;139:1177–83.
9 Lee H, Park SH, Shin EC. IL-15 in T-Cell Responses and Immunopathogenesis. *Immune Netw* 2024;24:e11.
10 Guo Y, Luan L, Patil NK, *et al*. Immunobiology of the IL-15/IL-15Rα complex as an antitumor and antiviral agent. *Cytokine Growth Factor Rev* 2017;38:10–21.
11 Zhang S, Zhao J, Bai X, *et al*. Biological effects of IL-15 on immune cells and its potential for the treatment of cancer. *Int Immunopharmacol* 2021;91:107318.
12 Ohaegbulam KC, Assal A, Lazar-Molnar E, *et al*. Human cancer immunotherapy with antibodies to the PD-1 and PD-L1 pathway. *Trends Mol Med* 2015;21:24–33.
13 Inman BA, Longo TA, Ramalingam S, *et al*. Atezolizumab: A PD-L1-Blocking Antibody for Bladder Cancer. *Clin Cancer Res* 2017;23:1886–90.
14 Shi W, Lv L, Liu N, *et al*. A novel anti-PD-L1/IL-15 immunocytokine overcomes resistance to PD-L1 blockade and elicits potent antitumor immunity. *Mol Ther* 2023;31:66–77.
15 Gurbatri CR, Lia I, Vincent R, *et al*. Engineered probiotics for local tumor delivery of checkpoint blockade nanobodies. *Sci Transl Med* 2020;12:eaax0876.
16 Chowdhury S, Castro S, Coker C, *et al*. Programmable bacteria induce durable tumor regression and systemic antitumor immunity. *Nat Med* 2019;25:1057–63.
17 Guo C, Liu J, Zhang Y. Current advances in bacteria-based cancer immunotherapy. *Eur J Immunol* 2024;54:e2350778.
18 Zhang Y, Huang R, Jiang Y, *et al*. The role of bacteria and its derived biomaterials in cancer radiotherapy. *Acta Pharm Sin B* 2023;13:4149–71.
19 Toyofuku M, Schild S, Kaparakis-Liaskos M, *et al*. Composition and functions of bacterial membrane vesicles. *Nat Rev Microbiol* 2023;21:415–30.
20 Li Z, Wang Y, Liu J, *et al*. Chemically and Biologically Engineered Bacteria-Based Delivery Systems for Emerging Diagnosis and Advanced Therapy. *Adv Mater Weinheim* 2021;33:e2102580.
21 Hernández A, Yager JA, Wilkie BN, *et al*. Evaluation of bovine cutaneous delayed-type hypersensitivity (DTH) to various test antigens and a mitogen using several adjuvants. *Vet Immunol Immunopathol* 2005;104:45–58.
22 Lange C, Aaby P, Behr MA, *et al*. 100 years of Mycobacterium bovis bacille Calmette-Guérin. *Lancet Infect Dis* 2022;22:e2–12.
23 Babjuk M, Burger M, Capoun O, *et al*. European Association of Urology Guidelines on Non-muscle-invasive Bladder Cancer (Ta, T1, and Carcinoma in Situ). *Eur Urol* 2022;81:75–94.
24 Ribi E, Milner KC, Granger DL, *et al*. Immunotherapy with nonviable microbial components. *Ann N Y Acad Sci* 1976;277:228–38.
25 Decroix G, Chastang C, Fichet D, *et al*. Adjuvant immunotherapy with nonviable Mycobacterium smegmatis in resected primary lung carcinoma. A randomized clinical trial of 219 patients. *Cancer* 1984;53:906–12.
26 Lamensans A, Chedid L, Lederer E, *et al*. Enhancement of immunity against murine syngeneic tumors by a fraction extracted from non-pathogenic mycobacteria. *Proc Natl Acad Sci U S A* 1975;72:3656–60.
27 Jeong H, Lee SY, Seo H, *et al*. Recombinant *Mycobacterium smegmatis* delivering a fusion protein of human macrophage migration inhibitory factor (MIF) and IL-7 exerts an anticancer effect by inducing an immune response against MIF in a tumor-bearing mouse model. *J Immunother Cancer* 2021;9:e003180.
28 Young SL, Murphy M, Zhu XW, *et al*. Cytokine-modified Mycobacterium smegmatis as a novel anticancer immunotherapy. *Int J Cancer* 2004;112:653–60.
29 Rich FJ, Kuhn S, Hyde EJ, *et al*. Induction of T cell responses and recruitment of an inflammatory dendritic cell subset following tumor immunotherapy with Mycobacterium smegmatis. *Cancer Immunol Immunother* 2012;61:2333–42.
30 Yarkoni E, Rapp HJ. Immunotherapy of experimental cancer by intralesional injection of emulsified nonliving mycobacteria: comparison of Mycobacterium bovis (BCG), Mycobacterium phlei, and Mycobacterium smegmatis. *Infect Immun* 1980;28:887–92.
31 Xu H, Shi M, Shao C, *et al*. Development of IL-15/IL-15Rα sushi domain-IgG4 Fc complexes in Pichia pastoris with potent activities and prolonged half-lives. *Microb Cell Fact* 2021;20:115.
32 Cheadle EJ, O'Donnell D, Selby PJ, *et al*. Closely related mycobacterial strains demonstrate contrasting levels of efficacy as antitumor vaccines and are processed for major histocompatibility complex class I presentation by multiple routes in dendritic cells. *Infect Immun* 2005;73:784–94.
33 Hovav A-H, Cayabyab MJ, Panas MW, *et al*. Rapid memory CD8+ T-lymphocyte induction through priming with recombinant Mycobacterium smegmatis. *J Virol* 2007;81:74–83.
34 Shen H, Aggarwal N, Wun KS, *et al*. Engineered microbial systems for advanced drug delivery. *Adv Drug Deliv Rev* 2022;187:114364.
35 Busatto C, Vianna JS, da Silva LV Junior, *et al*. Mycobacterium avium: an overview. *Tuberculosis (Edinb)* 2019;114:127–34.
36 Patel RB, Ye M, Carlson PM, *et al*. Development of an In Situ Cancer Vaccine via Combinational Radiation and Bacterial-Membrane-Coated Nanoparticles. *Adv Mater* 2019;31:e1902626.
37 Ma S, Caligiuri MA, Yu J. Harnessing IL-15 signaling to potentiate NK cell-mediated cancer immunotherapy. *Trends Immunol* 2022;43:833–47.
38 Ngwa W, Irabor OC, Schoenfeld JD, *et al*. Using immunotherapy to boost the abscopal effect. *Nat Rev Cancer* 2018;18:313–22.
39 Han X, Wei Q, Lv Y, *et al*. Ginseng-derived nanoparticles potentiate immune checkpoint antibody efficacy by reprogramming the cold tumor microenvironment. *Mol Ther* 2022;30:327–40.
40 Pulaski BA, Ostrand-Rosenberg S. Mouse 4T1 Breast Tumor Model. *CP in Immunology* 2000;39.
41 Taniura T, Iida Y, Kotani H, *et al*. Immunogenic chemotherapy in two mouse colon cancer models. *Cancer Sci* 2020;111:3527–39.
42 Becher B, Tugues S, Greter M. GM-CSF: From Growth Factor to Central Mediator of Tissue Inflammation. *Immunity* 2016;45:963–73.
43 Achuthan AA, Lee KMC, Hamilton JA. Targeting GM-CSF in inflammatory and autoimmune disorders. *Semin Immunol* 2021;54:101523.
44 Munsif M, Sweeney D, Leong TL, *et al*. Nebulised granulocyte-macrophage colony-stimulating factor (GM-CSF) in autoimmune

pulmonary alveolar proteinosis: a systematic review and meta-analysis. *Eur Respir Rev* 2023;32:230080.
45 Sweeney KA, Dao DN, Goldberg MF, *et al*. A recombinant Mycobacterium smegmatis induces potent bactericidal immunity against Mycobacterium tuberculosis. *Nat Med* 2011;17:1261–8.
46 Sparks IL, Derbyshire KM, Jacobs WR Jr, *et al*. Mycobacterium smegmatis: The Vanguard of Mycobacterial Research. *J Bacteriol* 2023;205:e00337-22.
47 Xie W, Wang L, Luo D, *et al*. *Mycobacterium smegmatis*, a Promising Vaccine Vector for Preventing TB and Other Diseases: Vaccinomics Insights and Applications. *Vaccines (Basel)* 2023;11:1302.
48 Cayabyab MJ, Hovav A-H, Hsu T, *et al*. Generation of CD8+ T-cell responses by a recombinant nonpathogenic Mycobacterium smegmatis vaccine vector expressing human immunodeficiency virus type 1 Env. *J Virol* 2006;80:1645–52.
49 Wang W, Xu H, Ye Q, *et al*. Systemic immune responses to irradiated tumours via the transport of antigens to the tumour periphery by injected flagellate bacteria. *Nat Biomed Eng* 2022;6:44–53.
50 Kitzmiller CE, Cheng T-Y, Prandi J, *et al*. Detergent-induced quantitatively limited formation of diacyl phosphatidylinositol dimannoside in Mycobacterium smegmatis. *J Lipid Res* 2024;65:100533.
51 Fan Y, Chen A, Zhu J, *et al*. Engineered lactococcus lactis intrapleural therapy promotes regression of malignant pleural effusion by enhancing antitumor immunity. *Cancer Lett* 2024;588:216777.